Article

Cell Reports

BET Inhibition-Induced GSK3β Feedback Enhances Lymphoma Vulnerability to PI3K Inhibitors

Graphical Abstract

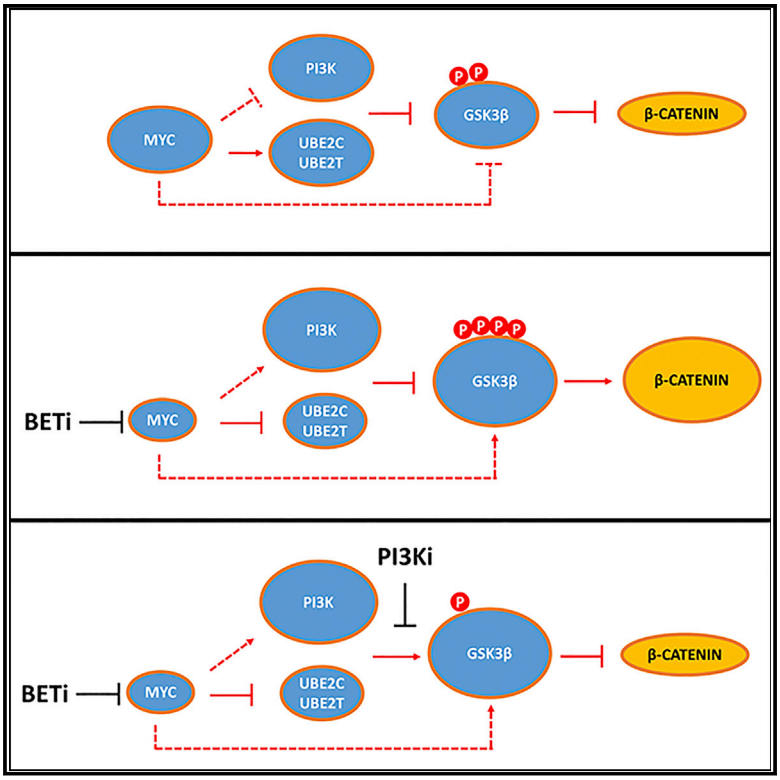

Authors

Enrico Derenzini, Patrizia Mondello, Tatiana Erazo, ..., Venkatraman E. Seshan, Ronald C. Hendrickson, Anas Younes

Correspondence

younesa@mskcc.org

In Brief

In this study, Derenzini et al. demonstrate that BET inhibitors enhance lymphoma vulnerability to PI3K inhibitors by inducing GSK3β feedback in a MYC-dependent manner and by downregulating E2-ubiquitin conjugating enzymes, which further enhance the feedback. These data provide the rationale for combining BET and PI3K inhibitors in lymphoma therapy.

Highlights

- BET inhibitors enhance lymphoma cell vulnerability to PI3K inhibitors
- BET inhibitors induce GSK3β feedback in a MYC-dependent manner
- Downregulation of UBE2C and UBE2T, induced by BET inhibitors, enhances GSK3β feedback
- BET inhibitors decrease MYC, UBE2C, and UBE2T and increase GSK3β S9 levels *in vivo*

Derenzini et al., 2018, Cell Reports *24*, 2155–2166
August 21, 2018
https://doi.org/10.1016/j.celrep.2018.07.055

CellPress

Cell Reports
Article

BET Inhibition-Induced GSK3β Feedback Enhances Lymphoma Vulnerability to PI3K Inhibitors

Enrico Derenzini,[1,2] Patrizia Mondello,[1] Tatiana Erazo,[1] Ana Portelinha,[1] Yuxuan Liu,[1] Mary Scallion,[1] Zahra Asgari,[1] John Philip,[3] Patrick Hilden,[4] Debora Valli,[2] Alessandra Rossi,[2] Hakim Djaballah,[5] Ouathek Ouerfelli,[6] Elisa de Stanchina,[7] Venkatraman E. Seshan,[4] Ronald C. Hendrickson,[3] and Anas Younes[1,8,9,*]
[1]Department of Medicine, Memorial Sloan Kettering Cancer Center, New York, NY, USA
[2]Oncohematology Unit, European Institute of Oncology, Milan, Italy
[3]Proteomics Core Facility, Memorial Sloan Kettering Cancer Center, New York, NY, USA
[4]Department of Epidemiology and Biostatistics, Memorial Sloan Kettering Cancer Center, New York, NY, USA
[5]High-Throughput Screening Core Facility, Memorial Sloan Kettering Cancer Center, New York, NY, USA
[6]Organic Synthesis Core Facility, Memorial Sloan Kettering Cancer, New York, NY, USA
[7]Antitumor Assessment Core, Memorial Sloan Kettering Cancer Center, New York, NY, USA
[8]Lymphoma Service, Memorial Sloan Kettering Cancer Center, New York, NY, USA
[9]Lead Contact
*Correspondence: younesa@mskcc.org
https://doi.org/10.1016/j.celrep.2018.07.055

SUMMARY

The phosphatidylinositol 3 kinase (PI3K)-glycogen synthase kinase β (GSK3β) axis plays a central role in MYC-driven lymphomagenesis, and MYC targeting with bromodomain and extraterminal protein family inhibitors (BETi) is a promising treatment strategy in lymphoma. In a high-throughput combinatorial drug screening experiment, BETi enhance the antiproliferative effects of PI3K inhibitors in a panel of diffuse large B cell lymphoma (DLBCL) and Burkitt lymphoma cell lines. BETi or MYC silencing upregulates several PI3K pathway genes and induces GSK3β S9 inhibitory phosphorylation, resulting in increased β-catenin protein abundance. Furthermore, BETi or *MYC* silencing increases GSK3β S9 phosphorylation levels and β-catenin protein abundance through downregulating the E2 ubiquitin conjugating enzymes UBE2C and UBE2T. In a mouse xenograft DLBCL model, BETi decrease MYC, UBE2C, and UBE2T and increase phospho-GSK3β S9 levels, enhancing the anti-proliferative effect of PI3K inhibitors. Our study reveals prosurvival feedbacks induced by BETi involving GSK3β regulation, providing a mechanistic rationale for combination strategies.

INTRODUCTION

Constitutive phosphoinositide 3-kinase (PI3K) activation plays a crucial role in the pathogenesis of MYC-driven lymphoma and is considered an attractive target for therapeutic intervention (Wendel et al., 2004; Sander et al., 2012; Pourdehnad et al., 2013). Furthermore, recent data highlight the function of B cell receptor (BCR)-PI3K-glycogen synthase kinase 3 (GSK3β) axis in supporting MYC-dependent transcriptional programs in lymphoma (Varano et al., 2017). GSK-3 is one of the main downstream targets of PI3K and regulates several signaling pathways involved in cellular metabolism, differentiation, immunity, and survival. GSK-3 phosphorylates a large number of proteins marking them for degradation, its activity being repressed by pro-survival phosphoinositide 3-kinase (PI3K)/protein kinase B (AKT) signaling. When AKT is activated, it phosphorylates the two isoforms of GSK-3 on their N terminus; GSK-3α at position S21 and GSK-3β at position S9. Because GSK phosphorylation is a major target of AKT, GSK-3β S9 phosphorylation is widely used to determine the activation status of the PI3K/AKT signaling pathway (Beurel et al., 2010, McCubrey et al., 2014; Walz et al., 2017).

The *MYC* transcription factor plays a central role in regulating cell growth, proliferation, and metabolism and is involved in the pathogenesis of a variety of lymphomas, including diffuse large B cell lymphoma (DLBCL) and Burkitt lymphoma (BL) (Dang, 2013, 2015; Green et al., 2012; Johnson et al., 2012). Although the development of drugs that can directly inhibit MYC protein function remains challenging, MYC-dependent transcription can be pharmacologically suppressed using compounds targeting bromodomain and extraterminal (BET) proteins, such as BRD2 and BRD4 (Delmore et al., 2011; Mertz et al., 2011). Accordingly, several BET inhibitors (BETi) are being developed for the treatment of a variety of MYC-driven cancers, including lymphoma (Delmore et al., 2011; Mertz et al., 2011; Chapuy et al., 2013; Boi et al., 2015; Trabucco et al., 2015). BET inhibition depletes enhancer and promoter-bound BRD4, leading to inhibition of *MYC* transcription and downregulation of MYC-dependent transcriptional programs (Delmore et al., 2011; Mertz et al., 2011; Chapuy et al., 2013; Lovén et al., 2013).

While BET inhibitors have been shown to disrupt several survival pathways, including suppressing the expression of MYC, reducing nuclear factor kappa-B (NF-κB) activity (Ceribelli et al., 2014), and suppressing E2F1-dependent transcriptional programs (Chapuy et al., 2013), they predominantly exerted cytostatic effects causing G1 cell-cycle arrest (Chapuy et al.,

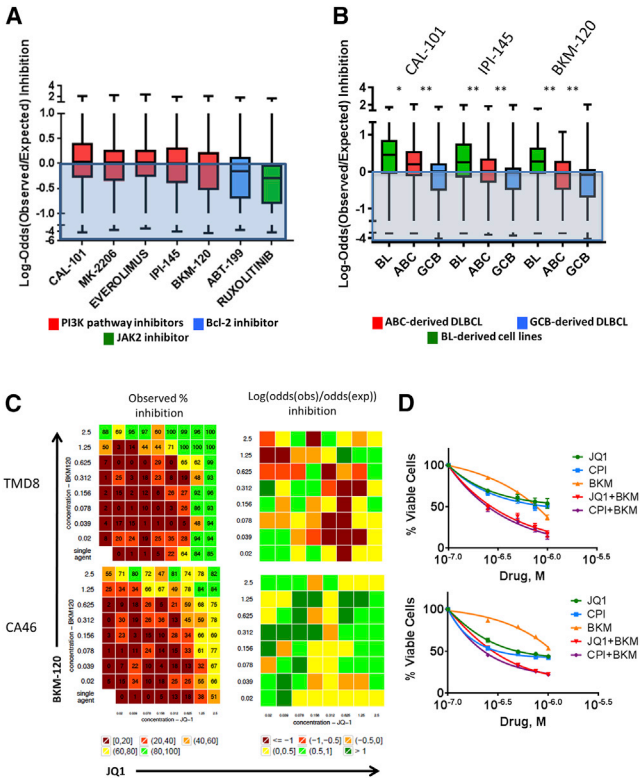

Figure 1. PI3K Pathway Inhibitors Enhance BET Inhibitor Activity in Lymphoma Cell Lines

(A) High-throughput screen of JQ1-based combinations with PI3K pathway inhibitors, the BCL2 inhibitor venetoclax (ABT-199), and the JAK2 inhibitor ruxolitinib. The boxplot graph summarizes the results of the combinatorial drug screening analyzed with the Bliss independence model in 12 cell lines treated for 72 hr with the indicated drug combinations. The y axis indicates the ratio between observed and expected inhibition in a log scale. The expected activity can be written as

$$P(Inh|A,B) = 1 - P(\overline{Inh}|A,B) = 1 - P(\overline{Inh}|A) \times P(\overline{Inh}|B) = 1 - [1 - P(Inh|A)] \times [1 - P(Inh|B)],$$

where A and B are the two drugs, and Inh $\overline{Inh}$ denote inhibited and not inhibited, respectively. Values above the "0" line indicate enhanced antiproliferative effects for JQ1-based combinations. See Data S1 and HTS statistical analysis in the Experimental Procedures for detailed information. See also Figures S1 and S2 for single agent activity data. Error bars represent minimum and maximum measured values.

(B) Boxplot graph summarizing the results of the combinatorial drug screening analyzed with the Bliss model according to the cell of origin. Error bars represent minimum and maximum measured values. Differences between groups (BL versus ABC and ABC versus GCB) were calculated with the Student's t test. *$p < 0.05$, **$p < 0.01$.

(C) Representative examples of combination experiments of JQ1 plus BKM-120 in TMD8 and CA-46 cells. Combination responses are examined using an 8 × 8 viability matrix which was measured after 72 hr post treatment. Full data are shown in Data S1.

(D) High-throughput results were confirmed by independent experiments using the MTS assay. Cells were incubated with increasing concentrations of BET inhibitors (JQ1 or CPI-203) and the PI3K inhibitor BKM-120 (0.25, 0.5, 0.75, 1 μM), and cell viability was assessed after 72 hr. Error bars represent SEM of triplicate experiments. Combination index data are provided in Figure S2D

2013). These observations prompted us to examine whether BET inhibition may induce feedback survival mechanisms preventing or attenuating its antitumor efficacy, and if so, whether blocking such feedback loops could be exploited for enhancing BET inhibitors activity through combination strategies. In this study, we report that BET inhibitors induced previously unknown MYC-dependent feedback loops involving the PI3K/GSK3 signaling. Accordingly, PI3K inhibitors (PI3Ki) enhanced the antiproliferative effects of BET inhibition in DLBCL and BL. Our findings provide mechanistic rationale for future combination strategies aimed at enhancing the efficacy of BET inhibitors in lymphoma.

RESULTS

BET Inhibitors Enhance Lymphoma Vulnerability to PI3K Inhibitors *In Vitro*

BET inhibitors (JQ1 and CPI-203) demonstrated a broad antiproliferative activity in a panel of 12 B cell lymphoma cell lines, including DLBCL of the germinal center B cell (GCB) and of the activated B cell (ABC) subtype, in addition to 2 BL cell lines (Figures S1A and S1B). The antiproliferative activity was observed irrespective of epigenetic modifying gene mutations (Figure S1B). The growth inhibition was predominantly due to G1 cell-cycle arrest (Figures S1C and S1D). As expected, JQ1 treatment downregulated *MYC* mRNA and decreased MYC protein levels (Figures S2A–S2C).

Recent investigations demonstrated the therapeutic value of targeting PI3K in ABC- and GCB-derived DLBCL (Erdmann et al., 2017; Paul et al., 2017), and several studies demonstrated oncogenic cooperation between MYC and PI3K (Wendel et al., 2004; Hoffman and Liebermann, 2008; Sander et al., 2012; Schmitz et al., 2012; Pourdehnad et al., 2013) and MYC and B cell lymphoma 2 (BCL-2) in lymphomagenesis (Strasser et al., 1990; Green et al., 2012; Johnson et al., 2012). Given the lack of effective cytotoxic activity of BET inhibitors despite their ability to downregulate MYC, we examined whether combining BET inhibitors with PI3K or BCL-2 inhibitors would produce enhanced antiproliferative effects. Using a high-throughput screening (HTS) approach, we combined BET inhibitors with drugs that inhibit PI3K/AKT/mTOR pathway activation at different signaling molecules, in addition to the selective BCL-2 inhibitor venetoclax (ABT-199). As shown in Figure 1A, inhibiting the PI3K pathway at different signaling molecules enhanced the effect of JQ1, whereas combinations with the BCL-2 inhibitor venetoclax had negligible effect on JQ1-induced antiproliferation.

The most favorable interactions between JQ1 and PI3Ki were observed in BL- and ABC-derived cell lines (Figure 1B). Detailed, individual matrices of 2 representative cell lines treated with JQ1 plus BKM-120 are shown in Figure 1C (complete data are provided in Data S1). These results were validated by independent experiments using the MTS cell proliferation assay, with two different BETi (JQ1 and CPI-203) producing similar results (Figure 1D). Combinations of BET and PI3K inhibitors showed more favorable interactions in cell lines harboring mutations of upstream components of the B cell receptor (BCR), Toll-like receptor (TLR), and PI3K pathway (*CD79B*, *MYD88*, *ID3*, *PTEN*, and *SGK1*) (Figure S2D).

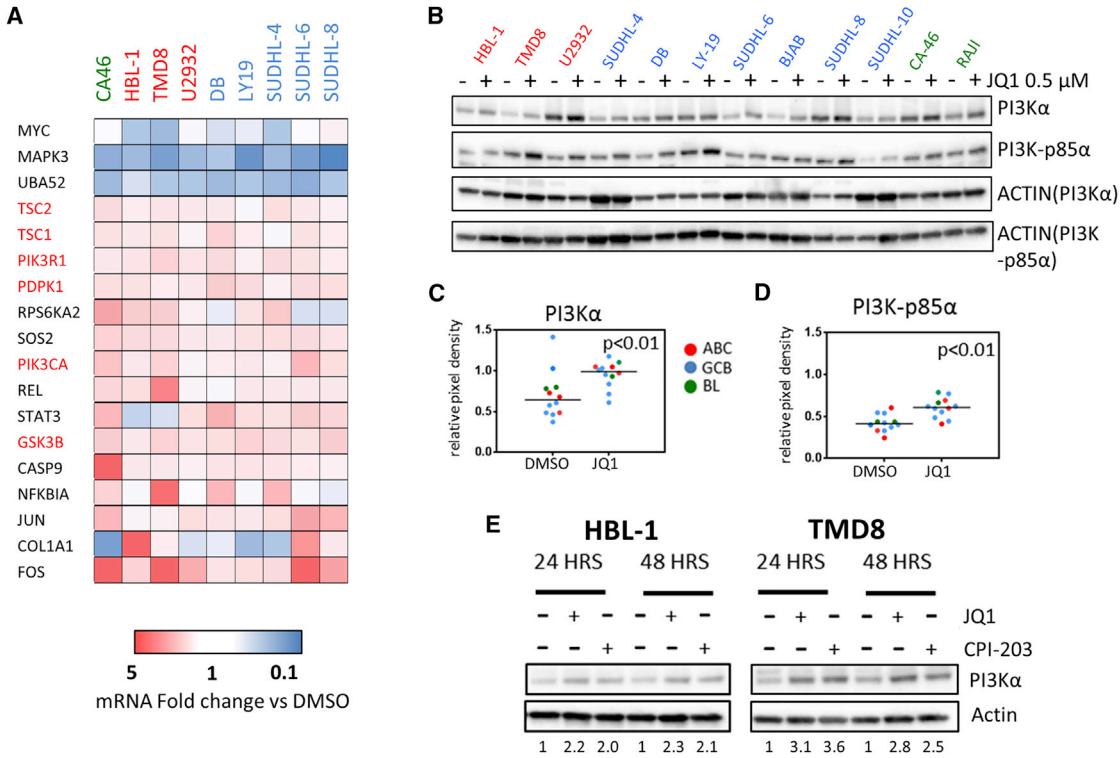

Figure 2. Effects of BET Inhibition on PI3K Pathway Gene Expression in DLBCL Cells

(A) Heatmap from one representative experiment showing the effect of JQ1 (0.5 μM for 24 hr) on PI3K pathway gene expression in multiple DLBCL/BL cell lines, as determined by a PCR pathway-directed array including genes belonging to PI3K pathway. MYC, and top down and upregulated genes (at least ±1.5 average fold change in 9 cell lines) are shown in the heatmap. Fold change values are depicted in a colorimetric scale from blue (low) to red (high) with respect to DMSO (control). Full data are shown in Figure S3.

(B) Representative western blot analysis confirming the effects of JQ1 (0.5 μM for 24 hr) on PI3Kα, PI3K-p85α (PIK3R1) protein levels DLBCL and BL cell lines.

(C) Scatterplots showing relative pixel density values of PI3Kα calculated versus actin. p values were calculated with the Wilcoxon rank test. Western blots images shown in (B) were analyzed with the ImageJ software.

(D) Scatterplots showing relative pixel density values of PI3K-p85α calculated versus actin. p values were calculated with the Wilcoxon rank test. Western blots images shown in (B) were analyzed with the ImageJ software.

(E) Representative western blots showing the effects of JQ1 and CPI-203 treatment (0.5 μM for 24 and 48 hr) on PI3Kα protein levels in HBL-1 and TMD8 cells, indicating similar class effects of JQ1 and CPI-203. Numbers indicate normalized PI3Kα levels relative to DMSO, calculated versus actin, and analyzed with the ImageJ software.

BET Inhibitors Induce GSK3β Feedback in Lymphoma

To better understand the molecular mechanisms underlying the favorable interactions between BET and PI3K inhibitors, we examined the regulatory effect of JQ1 on the transcription of genes involved in PI3K signaling and pathways, using a dedicated PCR pathway array platform (the gene list is available in the Supplemental Experimental Procedures). We found that JQ1 treatment (0.5 μM for 24 hr) upregulated the mRNA expression of several genes in the PI3K pathway, including *GSK3B* and upstream components of the pathway such as *PIK3CA* (PI3Kα) and *PIK3R1* (PI3K-p85α) (Figures 2A and S3), which was associated with an increase in protein levels in multiple cell lines (Figures 2B and 2C). Similar effects were observed using JQ1 and CPI-203, indicating a class effect (Figure 2D).These changes were associated with increased levels of phospho-GSK3β S9 in multiple cell lines (predominantly ABC and BL), as indicated by Luminex multiplex assay studies (Figure 3A). Validation of these data by western blot assay demonstrated increased pGSK3β S9 levels for up to 48 hr following treatment with JQ1 in TMD8 cells (Figure 3B). These findings were confirmed in BL cell lines and similar effects were observed using JQ1 or CPI-203 (Figure 3C). Although BET inhibitors increased total GSK3β levels in these cell lines (in line with the gene expression changes described in Figure 2A), the increased GSK3β S9 phosphorylation levels associated with increased protein abundance of its downstream target β-catenin are consistent with a "net" inhibitory effect of BET inhibitors on the GSK3β activity (Figure 3C). We could not see correlations between pAKT and pGSK3β levels (Figure 3C) suggesting that different kinases downstream of PI3K could mediate the observed GSK3β-feedback inhibition induced by BET inhibitors (reviewed in Beurel et al., 2015). Nuclear cytoplasmic fractionation experiments further corroborated our findings, as increased abundance of nuclear β-catenin was confirmed following treatment with either JQ1 or CPI-203 in ABC-derived DLBCL cell lines (Figure 3D). In line

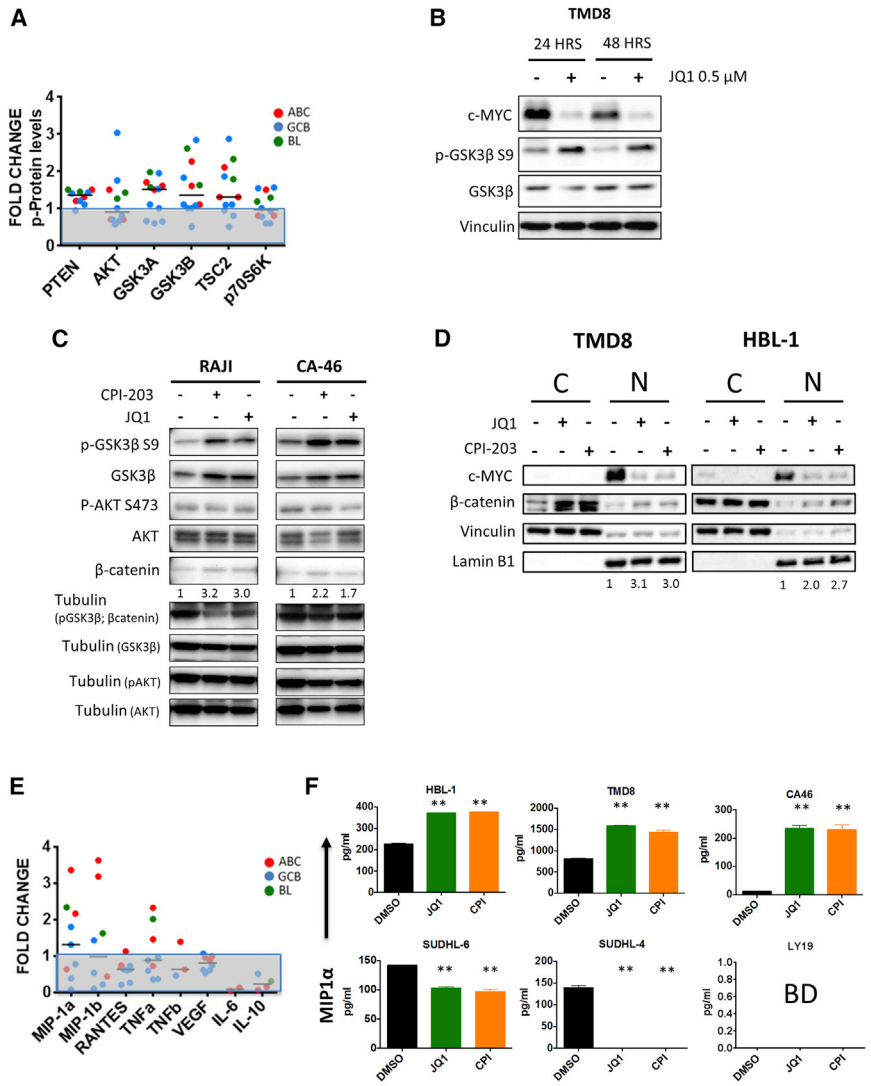

Figure 3. Effects of BET Inhibition on PI3K-GSK3β Signaling and Chemokine Secretion in DLBCL Cells

(A) Effect of JQ1 treatment (0.5 μM for 24 hr) on the phosphorylation level of PI3K pathway proteins including GSK3β (S9) in DLBCL and BL cell line panel, as determined by a luminex multiplex assay.

(B) Western blot confirming sustained effects of JQ1 on c-MYC, GSK3β (S9) and total GSK3β levels in TMD8 cells for up to 48 hr.

(C) Confirmatory western blots showing similar effects of JQ1 and CPI-203 (1 μM, 24 hr) on p-GSK3β S9, total GSK3β, and β-catenin levels in 2 BL cell lines (RAJI and CA-46). Numbers below β-catenin blots indicate fold-change of protein expression versus DMSO (normalized to the relative loading controls) evaluated by densitometry analysis using the ImageJ software.

(D) Nuclear-cytoplasmic fractionation experiments confirming increased nuclear β-catenin levels in ABC-derived DLBCL cell lines (TMD8, HBL-1) following treatment with BET inhibitors (JQ1 or CPI-203 0.5 μM for 24 hr). Vinculin and lamin B1 were used as loading controls for cytoplasmic and nuclear fractions, respectively. Numbers indicate fold-change of nuclear β-catenin protein expression versus DMSO (normalized to the relative loading controls), evaluated by densitometry analysis, using the ImageJ software. N, nuclear protein fractions; C, cytoplasmic protein fractions.

(E) Effect of JQ1 treatment (0.5 μM for 24 hr) on cytokine-chemokine levels as measured by a multiplex assay in 9 representative DLBCL cell lines of ABC and GCB origin (SUDHL-4, SUDHL-6, SUDHL-8, DB, BJAB, TMD8, HBL-1, and U2932), and 1 BL cell line (CA-46). As shown, JQ1 upregulated the PI3K-dependent chemokines MIP-1α and MIP1β mostly in ABC and BL cell lines. In some cell lines, cytokine levels were below detection. Results are shown as average fold change value of cytokine-chemokine concentration in cell culture supernatants (versus DMSO) of 3 independent experiments.

(F) Standard ELISA confirming significant MIP-1α upregulation in ABC-derived DLBCL cell lines (TMD8, HBL-1) and BL cell lines (CA-46) after treatment with JQ1 or CPI-203 0.5 μM for 24 hr. Error bars represent SEM of triplicate experiments. Differences between groups (JQ1 or CPI versus DMSO) were calculated with the Student's t test. *$p < 0.05$, **$p < 0.01$. BD (below detection).

with these data, we observed an increased production of the PI3K-dependent chemokines MIP-1α (CCL3) and MIP-1β (CCL4) after treatment with BET inhibitors (Figures 3E and 3F). These effects were more pronounced in ABC-derived (TMD8 and HBL-1) and BL cell lines (CA-46), compared to GCB-derived cell lines (SUDHL-6, SUDHL-4, and LY19) (Figures 3E and 3F) and were prevented by treatment with PI3K inhibitors (Figures 4A and 4B). Cell lines showing BETi-induced increase in pGSK3β S9 and/or MIP1α (CCL3) levels demonstrated more favorable interactions with PI3K inhibitors (Figure 4C). In order to confirm the importance of the induced GSK3β inhibitory feedback in determining the favorable interactions between BET and PI3K inhibitors, we generated inducible *GSK3β* short hairpin RNAs (shRNAs) in TMD8 cells using a tetracycline-dependent transactivation system, with the aim of creating a model of GSK3β inhibition that could not be reversed by the addition of PI3K inhibitors. *GSK3β* silencing did not have significant effects on cell proliferation and resulted in increased β-catenin protein abundance (Figure S4). In line with our hypothesis, a competitive proliferation assay demonstrated a significant proliferation advantage of GSK3β-depleted cells compared to scramble shRNA transduced cells after 72 hr incubation with BETi/PI3Ki combinations (Figures 4E and 4F). These data confirm that BETi-induced GSK3β feedback plays a major role in determining the favorable interactions between BET and PI3K inhibitors in DLBCL cells.

MYC Depletion Induces GSK3β Feedback in Lymphoma

To determine the role of MYC in the observed JQ1-induced PI3K/GSK3 feedback, we examined the effect of MYC silencing on PI3K pathway gene expression in the P-4936 B

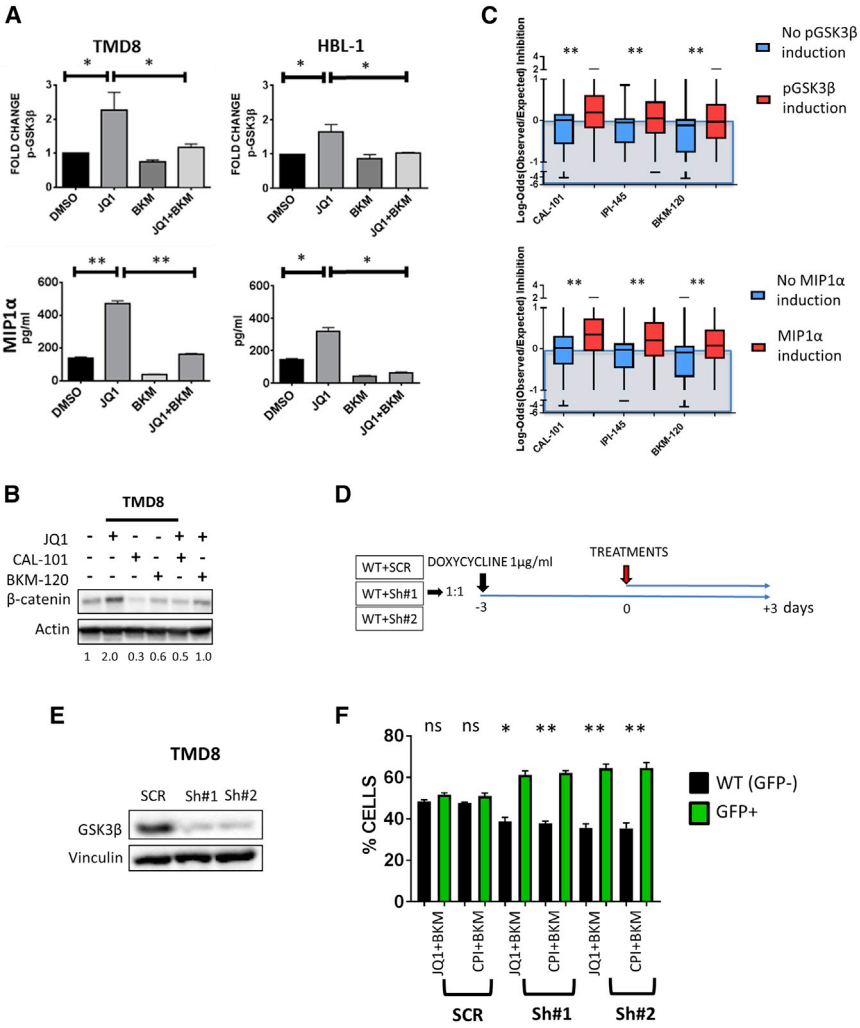

Figure 4. Effects of BET/PI3Ki Combinations on PI3K-GSK3 Signaling

(A) Effect of JQ1, BKM-120, and the combination on PI3K pathway activation in DLBCL cells. TMD8 and HBL-1 cells were incubated with JQ1 0.5 μM, BKM-120 0.5 μM, and the combination for 24 hr, and the effects on p-GSK3β S9 (top) and on MIP1α (CCL3) chemokine production (bottom) were assessed with Luminex multiplex assays. Error bars represent SEM of triplicate experiments. Differences between groups were calculated with the Student's t test. *$p < 0.05$, **$p < 0.01$.

(B) Representative western blot showing the effects of JQ1, CAL-101, BKM-120, and the combinations on β-catenin levels in TMD8 cells. Cells were incubated with JQ1 0.5 μM, CAL-101 1 μM, BKM-120 0.5 μM, and the combinations for 24 hr. Numbers indicate fold-change of β-catenin protein expression versus DMSO (normalized to actin levels), evaluated by densitometry analysis, using the ImageJ software.

(C) Boxplot graph summarizing the results of the combinatorial drug screening analyzed with the Bliss model according to on-treatment regulation of pGSK3β S9 phosphorylation by JQ1 (top) (as shown in the experiments represented in Figure 3A) and MIP1α (CCL3) production by JQ1 (bottom) (as shown in the experiments represented in Figures 3E and 3F). Error bars represent minimum and maximum measured values. Differences between groups were calculated with the Student's t test. *$p < 0.05$, **$p < 0.01$.

(D) Experimental design of the *GSK3β* shRNA cell growth completion assay experiments. 1:1 mixtures of wild-type (WT, GFP^-) cells and lentiviral shRNA-transduced (GFP^+) cells (WT+scramble [SCR], WT+Sh#1, and WT+Sh#2) were plated (250,000 cells/mL), pretreated with doxycycline (1 μg/mL) for 72 hr, and then treated with combinations of BET inhibitors (JQ1 and CPI-203) plus BKM-102 (0.5 μM). After 72 hr, the proportion of GFP^+ cells in each condition was evaluated by flow cytometry analysis.

(E) Western blot assay showing effective *GSK3β* silencing in TMD8 cells using 2 different inducible *GSK3β* shRNAs. Cells transduced with scramble (SCR), GSK3β Sh#1, or GSK3β Sh#2 were incubated with doxycycline (1 μg/mL) for 72 hr.

(F) Bar graphs showing increased proportion of GFP^+ cells following GSK3β depletion in TMD8 cells treated with combinations of BET and PI3K inhibitors, indicating a relative proliferative advantage of GSK3β-depleted cells in the presence of combinations of BET and PI3K inhibitors. Error bars represent SEM of triplicate experiments. Differences between groups (WT versus GFP^+ cells) were calculated with the Student's t test. *$p < 0.05$, **$p < 0.01$. Extended data are shown in Figure S4.

cell line, which carries a conditional, tetracycline-regulated (TET-OFF) *MYC* promoter (Pajic et al., 2000; Zeller et al., 2006). *MYC* silencing with doxycycline resulted in the time-dependent upregulation of several PI3K pathway genes, including *PIK3CA*, *PIK3CD*, and *GSK3β* (Figures 5A, 5B, and S5A). These changes were associated with increased levels of GSK3β and phospho-GSK3β S9 and with increased β-catenin protein abundance indicative of "net" inhibition of GSK3β activity, in addition to an increase in MIP1α levels in cell culture supernatants (Figures 5C, 5D, and S5B), therefore mirroring the effects of pharmacologic BET inhibition. Similarly, *MYC* silencing using small interfering RNA (siRNA) upregulated PI3K pathway gene expression in DLBCL cells (Figures 5E and 5F), and enhanced the antiproliferative effects of the PI3K inhibitor BKM-120 (Figure 5G). In line with these findings, a deep c-MYC downregulation correlated with a more favorable combinatory activity of JQ1 with PI3K inhibitors in DLBCL cell lines (Figure 5H). In summary, our data demonstrate that feedback upregulation of the PI3K pathway with consequent GSK3β feedback is a MYC-dependent event and provide a mechanistic rationale for combining BET inhibitors with PI3K inhibitors in DLBCL.

BET Inhibitors Regulate Protein Ubiquitination

Stable isotope labeling of amino acids in cell culture (SILAC)-based quantitative mass spectrometry was recently used to clarify the mechanism of the action of drugs that have complex biologic functions, such as lenalidomide (Krönke et al., 2014). Here, we applied SILAC-based quantitative mass spectrometry to two representative DLBCL cell lines treated with 0.5 μM JQ1

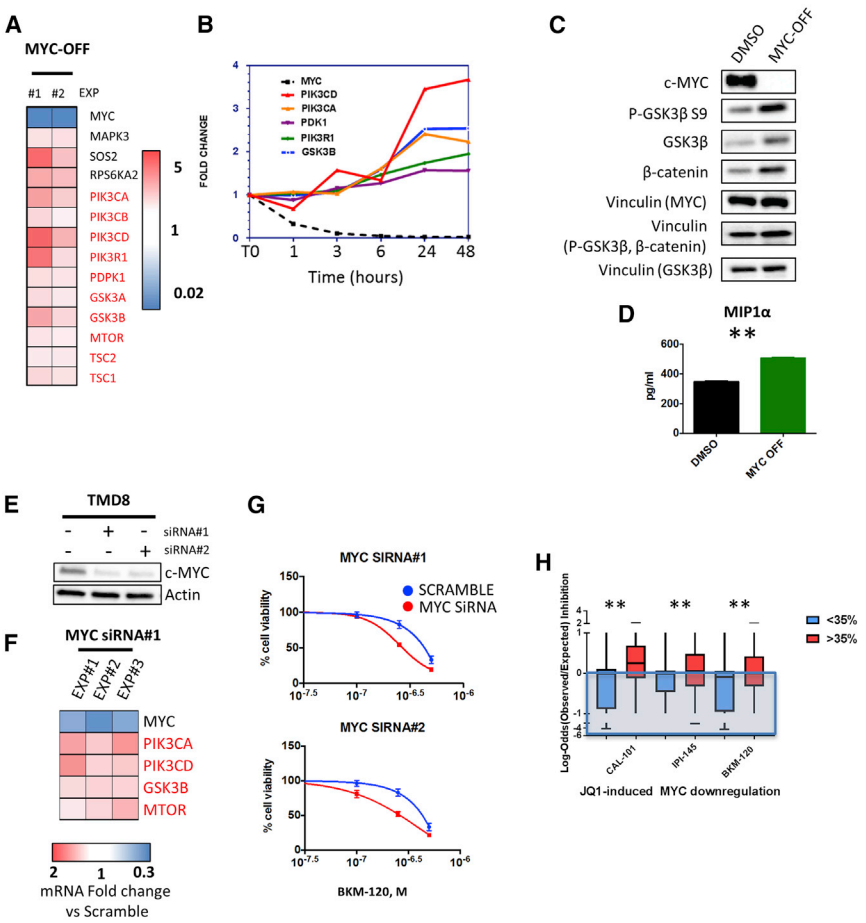

Figure 5. Effects of MYC Depletion on PI3K Pathway Gene Expression and Activation in Lymphoma Cells

(A) Effects of MYC silencing (MYC-OFF) for 24 hr on PI3K pathway-related genes, as determined by a PCR pathway-directed array in P-4936 cells. Fold change values obtained in 2 independent experiments are represented in a colorimetric scale from blue (low) to red (high). See also Figure S5A.

(B) Representative time course experiment showing changes in *PIK3CA*, *PIK3CD*, *PI3KR1*, *PDPK1*, and *GSK3B* gene expression levels in relation to *MYC* mRNA levels in P-4396 cells treated with doxycycline (1 μg/mL), assessed by PI3K pathway PCR-directed array.

(C) Western blot assay showing increased GSK3β protein abundance, enhanced p-GSK3β S9 phosphorylation, and increased β-catenin levels in P-4936 cells after 24 hr of *MYC* depletion (MYC-OFF). See also Figure S5B.

(D) Bar graph showing the effect of 24-hr MYC silencing (MYC-OFF) on MIP1α (CCL3) concentrations in cell culture supernatants of P-4936 cells, as detected by standard ELISA. Error bars represent SEM of triplicate experiments. Differences between groups were calculated with the Student's t test. *$p < 0.05$, **$p < 0.01$.

(E) Western blot showing the effects of the 2 different *MYC* siRNAs on MYC protein levels after 24 hr of incubation in TMD8 cells.

(F) Effects of *MYC* silencing by RNA interference (siRNA#1) on PI3K pathway gene expression in TMD8 cells. Fold change values obtained in 3 independent experiments with respect to scramble (SCR) siRNA (control) are shown.

(G) *MYC* silencing (with 2 different siRNAs) enhances the antiproliferative effect of the PI3K inhibitor BKM-120 (0.1, 0.25, 0.5 μM) in TMD8 cells at 48 hr. Viability data were normalized to the effect of *MYC* siRNA alone. Error bars represent SEM of triplicate experiments.

(H) Boxplot graph summarizing the results of the combinatorial drug screening analyzed with the Bliss model according to on-treatment regulation of MYC protein abundance at 24 hr by JQ1, as shown in the experiments represented in Figure S2B. The cut-off used in this plot (35% downregulation) corresponds to the median value of MYC downregulation calculated across all cell lines at 24 hr (Figure S2B). Error bars represent minimum and maximum measured values. Differences between groups were calculated with the Student's t test. *$p < 0.05$, **$p < 0.01$.

for 24 hr (HBL-1 of ABC origin and SUDHL-6 of GCB origin) (Figure 6A; Data S2). Pathway analysis using Ingenuity software showed that cell cycle, DNA damage response, nucleotide synthesis, and protein ubiquitination were among the top dysregulated cellular processes in both cell lines (Figures 6A and S6A). Of the 4,041 proteins that were detectable in both cell lines, only 10 proteins were commonly increased or decreased after treatment with JQ1 (Figures 6A and 6B). Three of top 5 downregulated proteins (UBE2C, UBE2T, and CDC20) belonged to the protein ubiquitination machinery (Figure 6B). These proteins are known to regulate the anaphase promoting complex/cyclosome (APC/C) ubiquitin E3 ligase (UBE2C and CDC20) and DNA damage response (UBE2T) (Rape and Kirschner, 2004; Buschhorn and Peters, 2006; Machida et al., 2006; Ueki et al., 2009; Williamson et al., 2009; Zhang et al., 2014). The effect of BET inhibitors (JQ1 and CPI-203) on UBE2C and UBE2T protein abundance was confirmed using western blotting in ABC (HBL-1 and TMD8) and GCB (SUDHL-6 and SUDHL-8) cell lines (Figure 6C).

To better understand the mechanisms and extent of regulation of protein ubiquitination machinery by BET inhibitors, we investigated the effect of JQ1 on gene expression levels of 84 genes spanning E1, E2, and E3 enzymes (Figure 6D; gene list available in the Supplemental Experimental Procedures). JQ1 treatment suppressed the expression of a wide range of E2-conjugating and E3-ligase enzymes (Figures 6D and S6B). Again, using the P-4936 human B cell lymphoma cell line, we found that doxycycline-induced MYC silencing resulted in downregulation of key E2 and E3 genes, including *UBE2C*, *UBE2T*, *SKP2*, and *UBE2S* (Figure 6E). The functional consequences of these findings were further investigated using gene silencing experiments. RNA interference for *UBE2C* and/or *UBE2T* in 2 ABC DLBCL cell lines resulted in increased GSK3β, phospho-GSK3β S9, and β-catenin protein levels (Figure 6F). Interestingly the effects of combined *UBE2C*/*UBE2T* silencing on GSK3β S9 phosphorylation were more pronounced compared to the effects of the single knockdowns, suggesting non-redundant functions of UBE2C

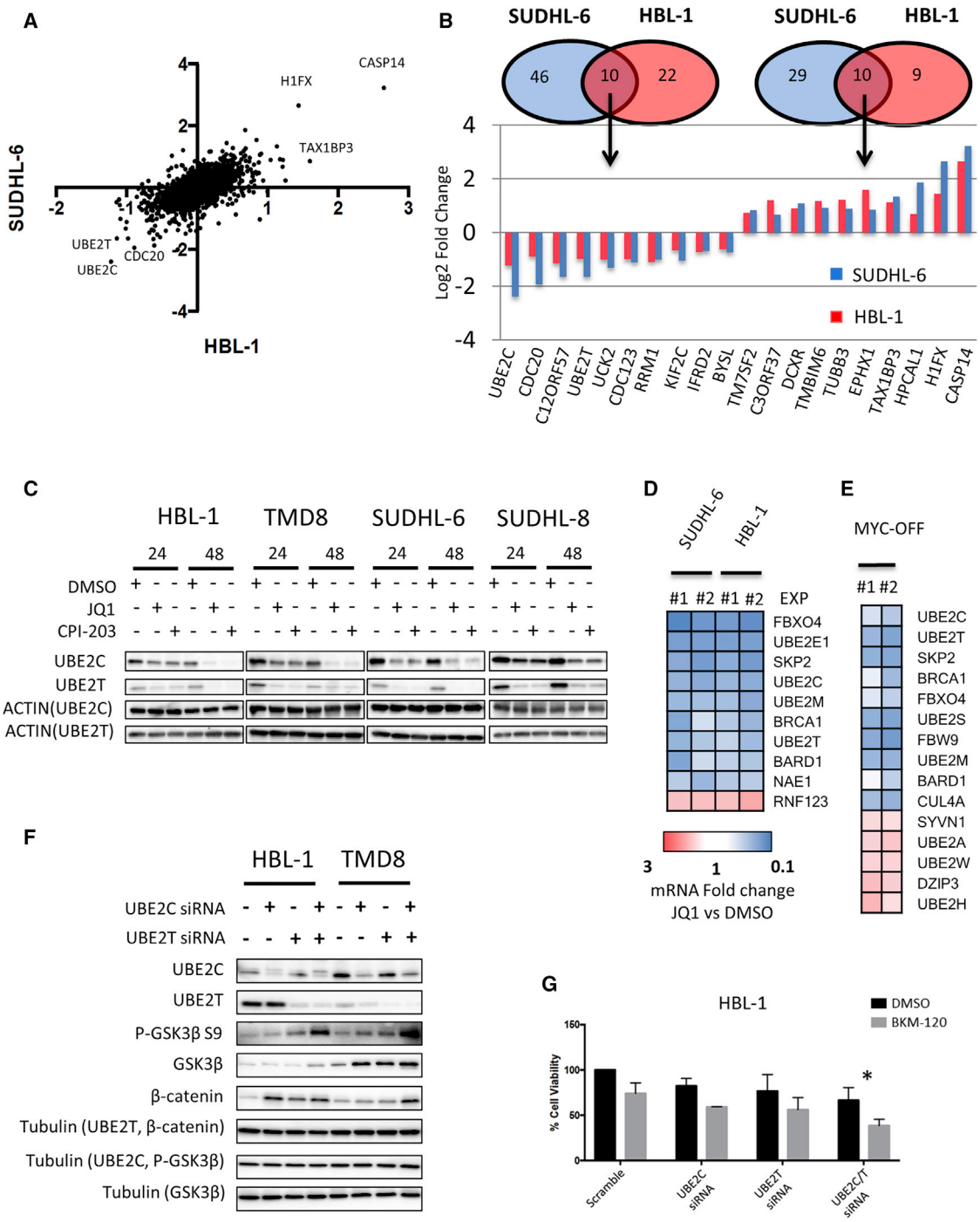

Figure 6. BETi-Mediated Regulation of the Ubiquitin System

(A) Scatterplot of quantitative proteomics data showing protein changes in HBL-1 (x axis) and SUDHL6-cells (y axis) in a log2 scale. Average log2 fold change of one forward and reverse experiment in HBL-1 and SUDHL-6 cells were used to generate the scatterplot. See also Figure S6A and Data S2.

(B) Venn diagram showing overlap of significantly up and downregulated proteins in HBL-1 (red) and SUDHL-6 cells (blue), and bar graph showing fold change in the top 10 commonly up- and downregulated proteins in HBL-1 (red) and SUDHL-6 cells (blue).

(C) Representative western blot showing marked decrease in UBE2C and UBE2T protein levels in 4 representative cell lines after 24 and 48 hr of incubation with 0.5 μM JQ1.

(D) Effects of JQ1 (0.5 μM for 24 hr) on ubiquitination pathways gene expression in HBL-1 and SUDHL-6 cells, as determined by PCR pathway-directed array. Genes commonly regulated in HBL-1 and SUDHL-6 cells by at least ±1.5-fold change are shown. Fold change values of JQ1-treated cells versus DMSO obtained in 2 independent experiments are represented in a colorimetric scale from blue (low) to red (high). See also Figure S6B.

(legend continued on next page)

and UBE2T in PI3K pathway regulation. In line with this data, combined UBE2C and UBE2T depletion enhanced the anti-lymphoma activity of the PI3K inhibitor BKM-120 in DLBCL cells, thus recapitulating the effects of BET inhibitors (Figure 6G).

Taken together, these data indicate that BET inhibitors may control the levels of GSK3β phosphorylation and β-catenin protein abundance by regulating ubiquitination pathways, and downregulation of E2 conjugating enzymes could be a relevant mechanism underlying the favorable interactions between BET and PI3K inhibitors.

BET Inhibition Increases DLBCL Vulnerability to PI3K Inhibition *In Vivo*

To determine whether the observed BET inhibitors-induced feedbacks are maintained *in vivo*, we examined the effect of CPI-203 on selected targets using a human DLBCL xenograft model. CPI-203 treatment (5 mg/kg given intraperitoneally [i.p.] twice daily) resulted in a modest inhibition of tumor growth (Figure 7A) without causing a significant weight loss (Figure S7A). At the molecular level, CPI-203 therapy resulted in downregulation of c-MYC, UBE2C, and UBE2T protein levels and in a trend toward increased GSK3β S9 phosphorylation (with 6 of 8 CPI-203-treated mice displaying relatively high p-GSK3β S9 levels versus only 3 of 8 mice in the control group) (Figures 7B–7D). In line with our findings, BET inhibition increased vulnerability to the PI3K inhibitor BKM-120 *in vivo*, with no significant weight loss (Figures 7E and S7B).

DISCUSSION

Our study provides insights on the complex biologic activity of BET inhibitors. While previous studies reported several mechanisms of anti-tumor activity of BET inhibitors in lymphoma (Chapuy et al., 2013; Ceribelli et al., 2014), our study describes prosurvival feedback mechanisms involving GSK3β. BET inhibitors downregulation of MYC leads to upregulation of PI3K pathway components and GSK3β inhibition. These molecular events were regulated by transcriptional and post-translational mechanisms (Figure 7F). Downregulation of MYC by BET inhibitors or genetic silencing of *MYC* resulted in the upregulation of several genes involved in regulating the PI3K pathway. This effect was associated with increased GSK3β S9 phosphorylation and beta-catenin protein abundance and with increased production of the PI3K-dependent chemokines MIP-1α and MIP-1β (Takahashi et al., 2015). Notably JQ1-induced inhibition of GSK3β and MIP1α increased production correlated with more favorable interactions between BET and PI3K inhibitors, confirming the functional relevance of these feedbacks and providing potential biomarkers for future clinical trials. These observations provided a mechanistic explanation for the favorable *in vitro* anti-lymphoma activity that we observed with the combination of BET inhibitors and several PI3K pathway inhibitors. Recently, small molecule inhibitors of the phosphatidylinositol 3-kinase pathway have been described to be active in DLBCL with different mechanisms according to the cell of origin (Erdmann et al., 2017; Paul et al., 2017). Our data also show differential efficacy of these combinations according to the cell of origin, with PI3Ki-based combinations being more active in the BL- and ABC-derived cell lines. Of note, recent data highlight the crucial role of BCR-dependent GSK3β inhibitory phosphorylation in maintaining fitness of MYC-driven lymphoma (Varano et al., 2017). Our observations of increased efficacy of PI3Ki-based combinations in ABC- and BL-derived cell lines harboring upstream BCR signaling mutations (*CD79B*, *ID3*, and *GNA13*) are in line with this model, as BETi-induced pGSK3β S9 accumulation could increase the vulnerability to PI3K inhibition in those cell lines relying on BCR-dependent GSK3β inhibition for survival. In line with this idea, shRNA-induced GSK3β depletion (that cannot be reversed by PI3K inhibitors) significantly decreased the efficacy of BET/PI3Ki combinations. Taken together, these data are consistent with a model where BET inhibition induces a GSK3β inhibitory feedback resulting in increased β-catenin signaling. At the same time, BET inhibitors, while inhibiting GSK3β activity, also increase GSK3β total protein levels. When a PI3K inhibitor is added, it reverses the GSK3β feedback unleashing a higher quantity of active GSK3β, thus resulting in enhanced antiproliferative effects. Additionally, a different mechanistic rationale for combining BETi with PI3Ki was recently reported in solid tumor preclinical models, suggesting that these mechanisms may be cell-type-specific (Stratikopoulos et al., 2015).

Previous studies focused on the transcriptional regulation by BET inhibitors of key oncogenes, such as *MYC*. Our quantitative proteomics experiments demonstrated that the biologic activity of BET inhibitors is also mediated through complex post-translational mechanisms involving the regulation of E2 and E3 enzymes leading to modulation of intracellular signaling pathways and increased phosphorylation of target proteins, such as GSK3β. Whether this is a cell-type-specific event is yet to be determined. We demonstrated that depletion of E2 enzymes induced by BET inhibition could contribute to the observed GSK3β feedback and to the increased β-catenin levels, and according to these observations, combined depletion of UBE2C and UBE2T enhanced the antiproliferative activity of PI3K inhibitors. However, Hu et al. (2016) described an inhibitory effect of UBE2C knockdown on PI3K activation in different tumor types, which could imply that E2 regulation of PI3K signaling is cell-type-specific. The human genome encodes 38 E2 ligase and

(E) Significantly regulated ubiquitination pathway genes (at least ±1.5-fold change) in P-4936 cells treated with doxycycline (1 μg/mL) (MYC-OFF) for 24 hr, as detected by PCR pathway-directed array. Fold change values obtained in 2 independent experiments are represented in a colorimetric scale from blue (low) to red (high).

(F) Representative western blot showing the effects of *UBE2C*, *UBE2T*, and combined *UBE2C plus UBE2T* silencing on GSK3β/β-catenin axis in lymphoma cells (2 ABC-derived DLBCL cell lines [TMD8 and HBL-1]) at 48 hr.

(G) Bar graphs showing the antiproliferative effects of Scramble, *UBE2C*, *UBE2T*, and combined *UBE2C/T* siRNAs plus or minus BKM-120 in HBL-1 cells. Combined *UBE2C/T* silencing significantly enhanced the antiproliferative effect of the PI3K inhibitor BKM-120 (0.5 μM) at 48 hr. Error bars represent SEM of triplicate experiments. Differences between groups were calculated with the Student's t test. *$p < 0.05$, **$p < 0.01$.

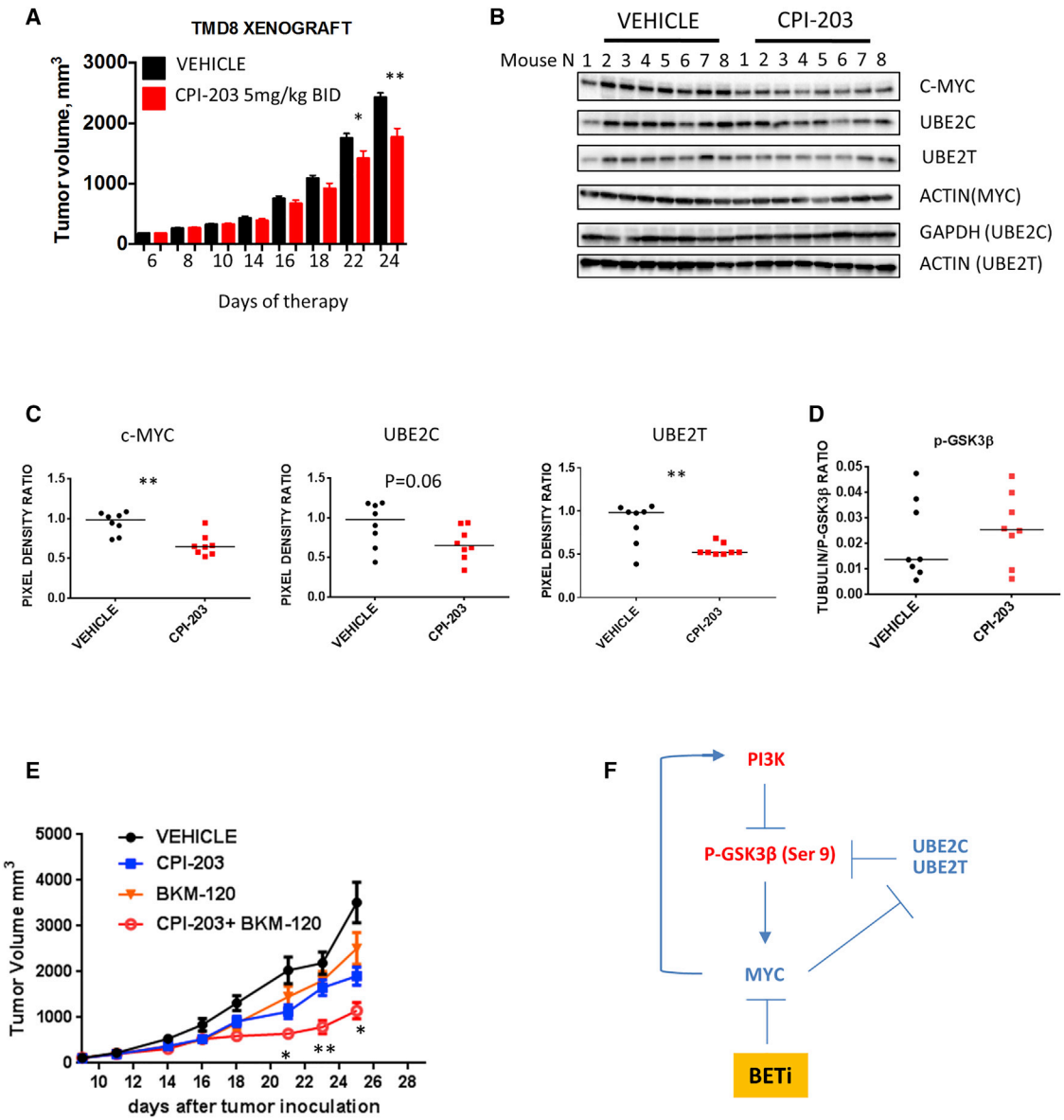

Figure 7. Antiproliferative Activity of BETi-PI3Ki Combinations *In Vivo*

(A) Human TMD8 cells were established as subcutaneous (s.c.) tumors in NSG mice and treated by i.p. injection with vehicle (n = 8) or the BET inhibitor CPI-203 (5 mg/kg BID) (n = 8) for 18 days. Tumor volume was measured 3 times per week. Error bars represent SEM. Differences between groups were calculated with the Student's t test. *p < 0.05, **p < 0.01.

(B) Western blot showing the *in vivo* effects of CPI-203 therapy on selected targets (MYC, UBE2C, and UBE2T).

(C) Scatterplots summarizing changes in expression levels of c-MYC, UBE2C, and UBE2T (as in B), analyzed in aggregate, and expressed as ratios of pixel densities between actin and protein of interest. Densitometry analysis was performed by using the ImageJ software. Differences between groups were calculated with the Wilcoxon rank test.*p < 0.05, **p < 0.01.

(D) *In vivo* effects of CPI-203 on p-GSK3β S9 phosphorylation in TMD8 xenografts. Proteins were extracted from tumor tissues and analyzed by Luminex multiplex assay. The expression levels of GSK3β S9 in mice bearing TMD8 xenografts treated with CPI-203 compared to vehicle were analyzed by Luminex multiplex assay and normalized to tubulin expression levels in each mouse.

(E) Combination experiment of CPI-203 and BKM-120 in TMD8 mouse xenografts. NSG mice were treated with vehicle (n = 8), the BET inhibitor CPI-203 (5 mg/kg twice daily i.p.) (n = 8), the PI3K inhibitor BKM-120 (15 mg/Kg/daily by oral gavage), and the combination (n = 8). Error bars represent SEM. Differences between groups were calculated with the Student's t test (CPI-203 versus combination). *p < 0.05, **p < 0.01. See also Figure S7.

(F) Model of interaction between BET inhibitors, the PI3K/GSK3β axis and ubiquitination pathways. Upon BET inhibition, MYC downregulation triggers negative feedbacks loops involving multiple PI3K pathway nodes, resulting in increased levels of phospho-GSK3β S9 and β-catenin signaling. Transcriptional down-regulation of the E2-conjugating enzymes UBE2C and UBE2T results in increased GSK3B phosphorylation, contributing to negative feedback regulation of the PI3K pathway.

more than 600 E3 ubiquitin ligases (Liu et al., 2015): lineage-dependent expression level of these enzymes may lead to lymphoid-restricted substrate specificity and ubiquitination mechanisms, which needs to be further explored.

In conclusion, our study described a feedback mechanism induced by BET inhibitors increasing vulnerability to PI3K inhibitors and established a framework for the development of combinatorial strategies to enhance BET inhibitors activity in DLBCL.

EXPERIMENTAL PROCEDURES

Cell Lines and Reagents

The human DLBCL-derived cell lines SUDHL-4, SUDHL-6, OCI-LY-19, and U-2932 were obtained from the DSMZ-German Collection of Microorganisms and Cell Cultures, Department of Human and Animal Cell Cultures (Braunschweig, Germany). DB, SUDHL-8, and SUDHL-10 and the BL cell lines RAJI and CA-46 were obtained from ATCC (American Type Culture Collection). The DLBCL-derived cell lines (HBL-1, TMD8, and BJAB) were provided by Dr. R.E. Davis (MD Anderson Cancer Center, Houston, TX). P-4936 cells (Pajic et al., 2000; Zeller et al., 2006) were provided by Dr. J. Zhang (Thompson lab, Memorial Sloan Kettering Cancer Center, New York, NY). Cell lines were fingerprinted at the Integrated Genomic Operation Core, (Memorial Sloan Kettering Cancer Center, New York, NY). Cell lines were cultured in RPMI 1640 medium supplemented with 10%–20% heat-inactivated fetal bovine serum (Hyclone, GE Healthcare Life Sciences [cat. #SH30396.03]), 1% L-glutamine, and penicillin-streptomycin in a humid environment of 5% CO_2 at 37°C. Mutations were annotated according to Cancer Cell Line Encyclopedia (https://www.broadinstitute.org/ccle/home) and Davis et al. (2010), Pasqualucci et al. (2011), Ngo et al. (2011), Fontan et al. (2012), and Zhang et al. (2013).

JQ1 was purchased from BPS Biosciences (San Diego, CA). The following compounds were purchased from Selleckchem (Houston, TX): CAL-101, BKM-120, IPI-145, Everolimus, MK-2206, ABT-199, and Ruxolitinib. Doxycycline was purchased from SIGMA. CPI-203 was purchased from Adooq Biosciences (Irvine, CA). Detailed information on western blot antibodies is provided in the Supplemental Information.

High-Throughput Screening Experiments

Combination Studies

For the synergy assessment studies, a compound matrix was prepared in which compound 1 at 10 μM was titrated against compound 2 at 2.5 μM in a doubling dilution series and transferred into a 1,536-well microtiter assay plate. Internal controls for each assay plate were dispensed as previously described. To start the assay, cells were seeded at 1,000 cells per well in 8 μL of complete RPMI medium and incubated for 2 days followed by 1 μL AB for an additional day at 37°C. Plates were imaged on the LEADseeker Multimodality Imaging System (GE Healthcare, Piscataway, NJ) and resulting files were deconvoluted to obtain fluorescence values associated with each drug.

Detailed information on single agent studies is available in the Supplemental Information.

HTS Statistical Analysis

To evaluate whether a drug combination shows synergy, we compared the observed activity of the combination at that level to the expected activity under Bliss independence model. By treating percent inhibition as a probability and using the product rule for the probability of independent events, the expected activity can be written as

$$P(Inh|A,\ B) = 1 - P(\overline{Inh}|A,\ B) = 1 - P(\overline{Inh}|A) \times P(\overline{Inh}|B) = 1 - [1 - P(Inh|A)] \times [1 - P(Inh|B)],$$

where A and B are the two drugs, andInh $\overline{Inh}$ denote inhibited and not inhibited, respectively (Feller, 1971; Tallarida, 2001). Detailed information is available in the Supplemental Information.

In Vitro Proliferation Assay

Cells were seeded in 96-well plates at 25,000 cells/100 μL/well with either vehicle (DMSO 0.1%) or increasing concentrations of drugs for 24, 48, and 72 hr. Cell viability was assessed by adding MTS reagent (Promega) to the culture medium at 1:5 dilution, according to manufacturer's instructions.

Luminex Multiplex Assays

Samples were run using dedicated kits (Millipore) on a Luminex MAGPIX machine. The effects of JQ1 on MYC levels were assessed with a Luminex multiplex assay (#48-617MAG, Millipore) according to the manufacturer's instructions. To assess the effects of JQ1 on phosphorylation levels of PI3K pathway components (PTEN S380, AKT S473, GSK3α S21, GSK3β S9, TSC2 S939, mTOR S2448, and P70S6K T412), protein lysates were examined with a Luminex multiplex assay (#48-611MAG Millipore), according to the manufacturer's instructions.

Each sample was run in triplicate, using 20 μg of total protein per sample, using the Luminex MAGPIX machine. Results were normalized to beta-tubulin expression levels, and beta-tubulin magnetic beads, and antibody was purchased from Millipore (#46-713MAG).

Mass Spectrometry Studies

Cell Culture, Lysis, and In Situ *Digestion*

Cells were grown as suspension cultures in RPMI media supplemented with 10% FBS and penicillin and streptomycin either unlabeled L-arginine (Arg0) and L-lysine (Lys0) at 50 mg/L or equimolar amounts of the isotopic variants [U-^{13}C6]-L-arginine (Arg10) and [U-^{13}C6]-L-lysine HCl L-lysine (Lys6) (Cambridge Isotope Laboratories). After five cell doublings in suspension flask, cells were >99% labeled with the isotopes. Cells were collected, lysed in RIPA buffer, quantitated for protein BCA, mixed at a 1:1 ratio, separated by SDS/PAGE, and stained with Simply Blue (Life Technologies), and 15 gel sections were excised with *in situ* trypsin digestion of polypeptides in each gel slice that was performed as previously described (Shevchenko et al., 2006). Detailed methods are available in the Supplemental Information.

Maxquant

All tandem mass spectrometry (MS/MS) samples were analyzed using MaxQuant (Max Planck Institute of Biochemistry, Martinsried, Germany; version 1.3.0.3) and Scaffold Q+S (Proteomesoftware, Portland, OR, version 4.4.1). Detailed description is available in the Supplemental Information.

Mass Spectrometry Data Analysis

5,444 proteins were initially identified. Proteins with a missing value in one or both of the 2 cell lines were removed, as were proteins where one replicate fold change value was ≥10 times the other. 4,041 proteins were then evaluable for the final analysis (see Data S2). Only proteins changing by at least 1.5-fold change in both forward and reverse experiments were considered as significantly deregulated. Pathway analysis was performed with the Ingenuity software (IPA) (QIAGEN). Additional details on data analysis are provided in the Supplemental Information.

Xenograft Studies

NSG mice (Jackson Laboratory) were used for *in vivo* studies and were cared for in accordance with guidelines approved by the Memorial Sloan Kettering Cancer Center Institutional Animal Care and Use Committee and Research Animal Resource Center, and in line with the ARRIVE guidelines (Kilkenny et al., 2010). Detailed descriptions of xenograft studies are provided in the Supplemental Information.

Detailed descriptions of pathway arrays and qPCR, siRNA, shRNA, western blot methods, nuclear-cytoplasmic fractionation, cytokine and chemokine detection, flow cytometry, mass spectrometry studies, and HTS statistics are available in the Supplemental Information.

This study was approved by the institutional review board.

Statistical Analysis

Procedures to determine the effects of certain conditions on cell proliferation and apoptosis were performed in 3 independent experiments. The two-tailed Student's t test and Wilcoxon rank test were used to estimate the statistical significance of differences between results from the 3 experiments. Significance was set at $p < 0.05$. The PRISM software was used for the statistical analyses.

Combination Index Calculation

Replicates Were Averaged for the Analysis.

The selected combinations were tested for nature of effect using the Chou-Talalay (CT) method (Chou, 2010), which enables quantification of drug outcomes as a combination index (CI); CI = 1 shows additivity, CI < 1 shows synergism, and CI > 1 shows antagonism.

Data Availability

Proteomics data generated or analyzed during this study are included in this published article (and its supplemental information files). The raw proteomics data reported in this paper are also publicly available at the Peptide Atlas website (https://db.systemsbiology.net/sbeams/cgi/PeptideAtlas/PASS_View?identifier=PASS01217). Original uncropped western blots are available at the Mendeley database: https://doi.org/10.17632/px94fdcpvz.1.

SUPPLEMENTAL INFORMATION

Supplemental Information includes Supplemental Experimental Procedures, seven figures, and two data files and can be found with this article online at https://doi.org/10.1016/j.celrep.2018.07.055.

ACKNOWLEDGMENTS

This work was supported in part by the MSK SPORE in lymphoma (P50 CA192937-01A1 to A.Y. and V.E.S.), the Vogelstein Fund for Lymphoma Research (to A.Y.), and the Memorial Sloan Kettering Cancer Center Core (P30 CA008748).

AUTHOR CONTRIBUTIONS

E.D., P.M., T.E., A.P., H.D., E.d.S., R.C.H., and A.Y. designed the experiments. E.D., P.M., T.E., A.P., H.D., Y.L., M.S., Z.A., J.P., D.V., A.R., O.O., P.H., and V.E.S. performed experiments and analyzed data. E.d.S. supervised *in vivo* experiments. E.D., P.M., T.E., and A.Y. wrote the paper.

DECLARATION OF INTERESTS

The authors declare no competing interests.

Received: February 20, 2018
Revised: June 1, 2018
Accepted: July 16, 2018
Published: August 21, 2018

REFERENCES

Beurel, E., Michalek, S.M., and Jope, R.S. (2010). Innate and adaptive immune responses regulated by glycogen synthase kinase-3 (GSK3). Trends Immunol. *31*, 24–31.

Beurel, E., Grieco, S.F., and Jope, R.S. (2015). Glycogen synthase kinase-3 (GSK3): regulation, actions, and diseases. Pharmacol. Ther. *148*, 114–131.

Boi, M., Gaudio, E., Bonetti, P., Kwee, I., Bernasconi, E., Tarantelli, C., Rinaldi, A., Testoni, M., Cascione, L., Ponzoni, M., et al. (2015). The BET bromodomain inhibitor OTX015 affects pathogenetic pathways in preclinical B-cell tumor models and synergizes with targeted drugs. Clin. Cancer Res. *21*, 1628–1638.

Buschhorn, B.A., and Peters, J.M. (2006). How APC/C orders destruction. Nat. Cell Biol. *8*, 209–211.

Ceribelli, M., Kelly, P.N., Shaffer, A.L., Wright, G.W., Xiao, W., Yang, Y., Mathews Griner, L.A., Guha, R., Shinn, P., Keller, J.M., et al. (2014). Blockade of oncogenic IκB kinase activity in diffuse large B-cell lymphoma by bromodomain and extraterminal domain protein inhibitors. Proc. Natl. Acad. Sci. USA *111*, 11365–11370.

Chapuy, B., McKeown, M.R., Lin, C.Y., Monti, S., Roemer, M.G., Qi, J., Rahl, P.B., Sun, H.H., Yeda, K.T., Doench, J.G., et al. (2013). Discovery and characterization of super-enhancer-associated dependencies in diffuse large B cell lymphoma. Cancer Cell *24*, 777–790.

Chou, T.C. (2010). Drug combination studies and their synergy quantification using the Chou-Talalay method. Cancer Res. *70*, 440–446.

Dang, C.V. (2013). MYC, metabolism, cell growth, and tumorigenesis. Cold Spring Harb. Perspect. Med. *3*, a014217.

Dang, C.V. (2015). Web of the extended Myc network captures metabolism for tumorigenesis. Cancer Cell *27*, 160–162.

Davis, R.E., Ngo, V.N., Lenz, G., Tolar, P., Young, R.M., Romesser, P.B., Kohlhammer, H., Lamy, L., Zhao, H., Yang, Y., et al. (2010). Chronic active B-cell-receptor signalling in diffuse large B-cell lymphoma. Nature *463*, 88–92.

Delmore, J.E., Issa, G.C., Lemieux, M.E., Rahl, P.B., Shi, J., Jacobs, H.M., Kastritis, E., Gilpatrick, T., Paranal, R.M., Qi, J., et al. (2011). BET bromodomain inhibition as a therapeutic strategy to target c-Myc. Cell *146*, 904–917.

Erdmann, T., Klener, P., Lynch, J.T., Grau, M., Vočková, P., Molinsky, J., Tuskova, D., Hudson, K., Polanska, U.M., Grondine, M., et al. (2017). Sensitivity to PI3K and AKT inhibitors is mediated by divergent molecular mechanisms in subtypes of DLBCL. Blood *130*, 310–322.

Feller, W. (1971). An Introduction to Probability Theory and Its Applications (New York, NY: John Wiley&Sons).

Fontan, L., Yang, C., Kabaleeswaran, V., Volpon, L., Osborne, M.J., Beltran, E., Garcia, M., Cerchietti, L., Shaknovich, R., Yang, S.N., et al. (2012). MALT1 small molecule inhibitors specifically suppress ABC-DLBCL in vitro and in vivo. Cancer Cell *22*, 812–824.

Green, T.M., Young, K.H., Visco, C., Xu-Monette, Z.Y., Orazi, A., Go, R.S., Nielsen, O., Gadeberg, O.V., Mourits-Andersen, T., Frederiksen, M., et al. (2012). Immunohistochemical double-hit score is a strong predictor of outcome in patients with diffuse large B-cell lymphoma treated with rituximab plus cyclophosphamide, doxorubicin, vincristine, and prednisone. J. Clin. Oncol. *30*, 3460–3467.

Hoffman, B., and Liebermann, D.A. (2008). Apoptotic signaling by c-MYC. Oncogene *27*, 6462–6472.

Hu, W., Xiao, L., Cao, C., Hua, S., and Wu, D. (2016). UBE2T promotes nasopharyngeal carcinoma cell proliferation, invasion, and metastasis by activating the AKT/GSK3β/β-catenin pathway. Oncotarget *7*, 15161–15172.

Johnson, N.A., Slack, G.W., Savage, K.J., Connors, J.M., Ben-Neriah, S., Rogic, S., Scott, D.W., Tan, K.L., Steidl, C., Sehn, L.H., et al. (2012). Concurrent expression of MYC and BCL2 in diffuse large B-cell lymphoma treated with rituximab plus cyclophosphamide, doxorubicin, vincristine, and prednisone. J. Clin. Oncol. *30*, 3452–3459.

Kilkenny, C., Browne, W.J., Cuthill, I.C., Emerson, M., and Altman, D.G. (2010). Improving bioscience research reporting: the ARRIVE guidelines for reporting animal research. PLoS Biol. *8*, e1000412.

Krönke, J., Udeshi, N.D., Narla, A., Grauman, P., Hurst, S.N., McConkey, M., Svinkina, T., Heckl, D., Comer, E., Li, X., et al. (2014). Lenalidomide causes selective degradation of IKZF1 and IKZF3 in multiple myeloma cells. Science *343*, 301–305.

Liu, J., Shaik, S., Dai, X., Wu, Q., Zhou, X., Wang, Z., and Wei, W. (2015). Targeting the ubiquitin pathway for cancer treatment. Biochim. Biophys. Acta *1855*, 50–60.

Lovén, J., Hoke, H.A., Lin, C.Y., Lau, A., Orlando, D.A., Vakoc, C.R., Bradner, J.E., Lee, T.I., and Young, R.A. (2013). Selective inhibition of tumor oncogenes by disruption of super-enhancers. Cell *153*, 320–334.

Machida, Y.J., Machida, Y., Chen, Y., Gurtan, A.M., Kupfer, G.M., D'Andrea, A.D., and Dutta, A. (2006). UBE2T is the E2 in the Fanconi anemia pathway and undergoes negative autoregulation. Mol. Cell *23*, 589–596.

McCubrey, J.A., Steelman, L.S., Bertrand, F.E., Davis, N.M., Abrams, S.L., Montalto, G., D'Assoro, A.B., Libra, M., Nicoletti, F., Maestro, R., et al. (2014). Multifaceted roles of GSK-3 and Wnt/β-catenin in hematopoiesis and leukemogenesis: opportunities for therapeutic intervention. Leukemia *28*, 15–33.

Mertz, J.A., Conery, A.R., Bryant, B.M., Sandy, P., Balasubramanian, S., Mele, D.A., Bergeron, L., and Sims, R.J., 3rd. (2011). Targeting MYC dependence in

cancer by inhibiting BET bromodomains. Proc. Natl. Acad. Sci. USA *108*, 16669–16674.

Ngo, V.N., Young, R.M., Schmitz, R., Jhavar, S., Xiao, W., Lim, K.H., Kohlhammer, H., Xu, W., Yang, Y., Zhao, H., et al. (2011). Oncogenically active MYD88 mutations in human lymphoma. Nature *470*, 115–119.

Pajic, A., Spitkovsky, D., Christoph, B., Kempkes, B., Schuhmacher, M., Staege, M.S., Brielmeier, M., Ellwart, J., Kohlhuber, F., Bornkamm, G.W., et al. (2000). Cell cycle activation by c-myc in a Burkitt lymphoma model cell line. Int. J. Cancer *87*, 787–793.

Pasqualucci, L., Dominguez-Sola, D., Chiarenza, A., Fabbri, G., Grunn, A., Trifonov, V., Kasper, L.H., Lerach, S., Tang, H., Ma, J., et al. (2011). Inactivating mutations of acetyltransferase genes in B-cell lymphoma. Nature *471*, 189–195.

Paul, J., Soujon, M., Wengner, A.M., Zitzmann-Kolbe, S., Sturz, A., Haike, K., Keng Magdalene, K.H., Tan, S.H., Lange, M., Tan, S.Y., et al. (2017). Simultaneous inhibition of PI3Kδ and PI3Kα induces ABC-DLBCL regression by blocking BCR-dependent and -independent activation of NF-κB and AKT. Cancer Cell *31*, 64–78.

Pourdehnad, M., Truitt, M.L., Siddiqi, I.N., Ducker, G.S., Shokat, K.M., and Ruggero, D. (2013). Myc and mTOR converge on a common node in protein synthesis control that confers synthetic lethality in Myc-driven cancers. Proc. Natl. Acad. Sci. USA *110*, 11988–11993.

Rape, M., and Kirschner, M.W. (2004). Autonomous regulation of the anaphase-promoting complex couples mitosis to S-phase entry. Nature *432*, 588–595.

Sander, S., Calado, D.P., Srinivasan, L., Köchert, K., Zhang, B., Rosolowski, M., Rodig, S.J., Holzmann, K., Stilgenbauer, S., Siebert, R., et al. (2012). Synergy between PI3K signaling and MYC in Burkitt lymphomagenesis. Cancer Cell *22*, 167–179.

Schmitz, R., Young, R.M., Ceribelli, M., Jhavar, S., Xiao, W., Zhang, M., Wright, G., Shaffer, A.L., Hodson, D.J., Buras, E., et al. (2012). Burkitt lymphoma pathogenesis and therapeutic targets from structural and functional genomics. Nature *490*, 116–120.

Shevchenko, A., Tomas, H., Havlis, J., Olsen, J.V., and Mann, M. (2006). In-gel digestion for mass spectrometric characterization of proteins and proteomes. Nat. Protoc. *1*, 2856–2860.

Strasser, A., Harris, A.W., Bath, M.L., and Cory, S. (1990). Novel primitive lymphoid tumours induced in transgenic mice by cooperation between myc and bcl-2. Nature *348*, 331–333.

Stratikopoulos, E.E., Dendy, M., Szabolcs, M., Khaykin, A.J., Lefebvre, C., Zhou, M.M., and Parsons, R. (2015). Kinase and BET inhibitors together clamp inhibition of PI3K signaling and overcome resistance to therapy. Cancer Cell *27*, 837–851.

Takahashi, K., Sivina, M., Hoellenriegel, J., Oki, Y., Hagemeister, F.B., Fayad, L., Romaguera, J.E., Fowler, N., Fanale, M.A., Kwak, L.W., et al. (2015). CCL3 and CCL4 are biomarkers for B cell receptor pathway activation and prognostic serum markers in diffuse large B cell lymphoma. Br. J. Haematol. *171*, 726–735.

Tallarida, R.J. (2001). Drug synergism: its detection and applications. J. Pharmacol. Exp. Ther. *298*, 865–872.

Trabucco, S.E., Gerstein, R.M., Evens, A.M., Bradner, J.E., Shultz, L.D., Greiner, D.L., and Zhang, H. (2015). Inhibition of bromodomain proteins for the treatment of human diffuse large B-cell lymphoma. Clin. Cancer Res. *21*, 113–122.

Ueki, T., Park, J.H., Nishidate, T., Kijima, K., Hirata, K., Nakamura, Y., and Katagiri, T. (2009). Ubiquitination and downregulation of BRCA1 by ubiquitin-conjugating enzyme E2T overexpression in human breast cancer cells. Cancer Res. *69*, 8752–8760.

Varano, G., Raffel, S., Sormani, M., Zanardi, F., Lonardi, S., Zasada, C., Perucho, L., Petrocelli, V., Haake, A., Lee, A.K., et al. (2017). The B-cell receptor controls fitness of MYC-driven lymphoma cells via GSK3β inhibition. Nature *546*, 302–306.

Walz, A., Ugolkov, A., Chandra, S., Kozikowski, A., Carneiro, B.A., O'Halloran, T.V., Giles, F.J., Billadeau, D.D., and Mazar, A.P. (2017). Molecular pathways: revisiting glycogen synthase kinase-3β as a target for the treatment of cancer. Clin. Cancer Res. *23*, 1891–1897.

Wendel, H.G., De Stanchina, E., Fridman, J.S., Malina, A., Ray, S., Kogan, S., Cordon-Cardo, C., Pelletier, J., and Lowe, S.W. (2004). Survival signalling by Akt and eIF4E in oncogenesis and cancer therapy. Nature *428*, 332–337.

Williamson, A., Wickliffe, K.E., Mellone, B.G., Song, L., Karpen, G.H., and Rape, M. (2009). Identification of a physiological E2 module for the human anaphase-promoting complex. Proc. Natl. Acad. Sci. USA *106*, 18213–18218.

Zeller, K.I., Zhao, X., Lee, C.W., Chiu, K.P., Yao, F., Yustein, J.T., Ooi, H.S., Orlov, Y.L., Shahab, A., Yong, H.C., et al. (2006). Global mapping of c-Myc binding sites and target gene networks in human B cells. Proc. Natl. Acad. Sci. USA *103*, 17834–17839.

Zhang, J., Wan, L., Dai, X., Sun, Y., and Wei, W. (2014). Functional characterization of Anaphase Promoting Complex/Cyclosome (APC/C) E3 ubiquitin ligases in tumorigenesis. Biochim. Biophys. Acta *1845*, 277–293.

Zhang, J., Grubor, V., Love, C.L., Banerjee, A., Richards, K.L., Mieczkowski, P.A., Dunphy, C., Choi, W., Au, W.Y., Srivastava, G., et al. (2013). Genetic heterogeneity of diffuse large B-cell lymphoma. Proc. Natl. Acad. Sci. USA *110*, 1398–1403.

Cell Reports, Volume *24*

Supplemental Information

BET Inhibition-Induced GSK3β Feedback Enhances Lymphoma Vulnerability to PI3K Inhibitors

Enrico Derenzini, Patrizia Mondello, Tatiana Erazo, Ana Portelinha, Yuxuan Liu, Mary Scallion, Zahra Asgari, John Philip, Patrick Hilden, Debora Valli, Alessandra Rossi, Hakim Djaballah, Ouathek Ouerfelli, Elisa de Stanchina, Venkatraman E. Seshan, Ronald C. Hendrickson, and Anas Younes

Supplementary information

Supplemental figures and legends

Fig. S1

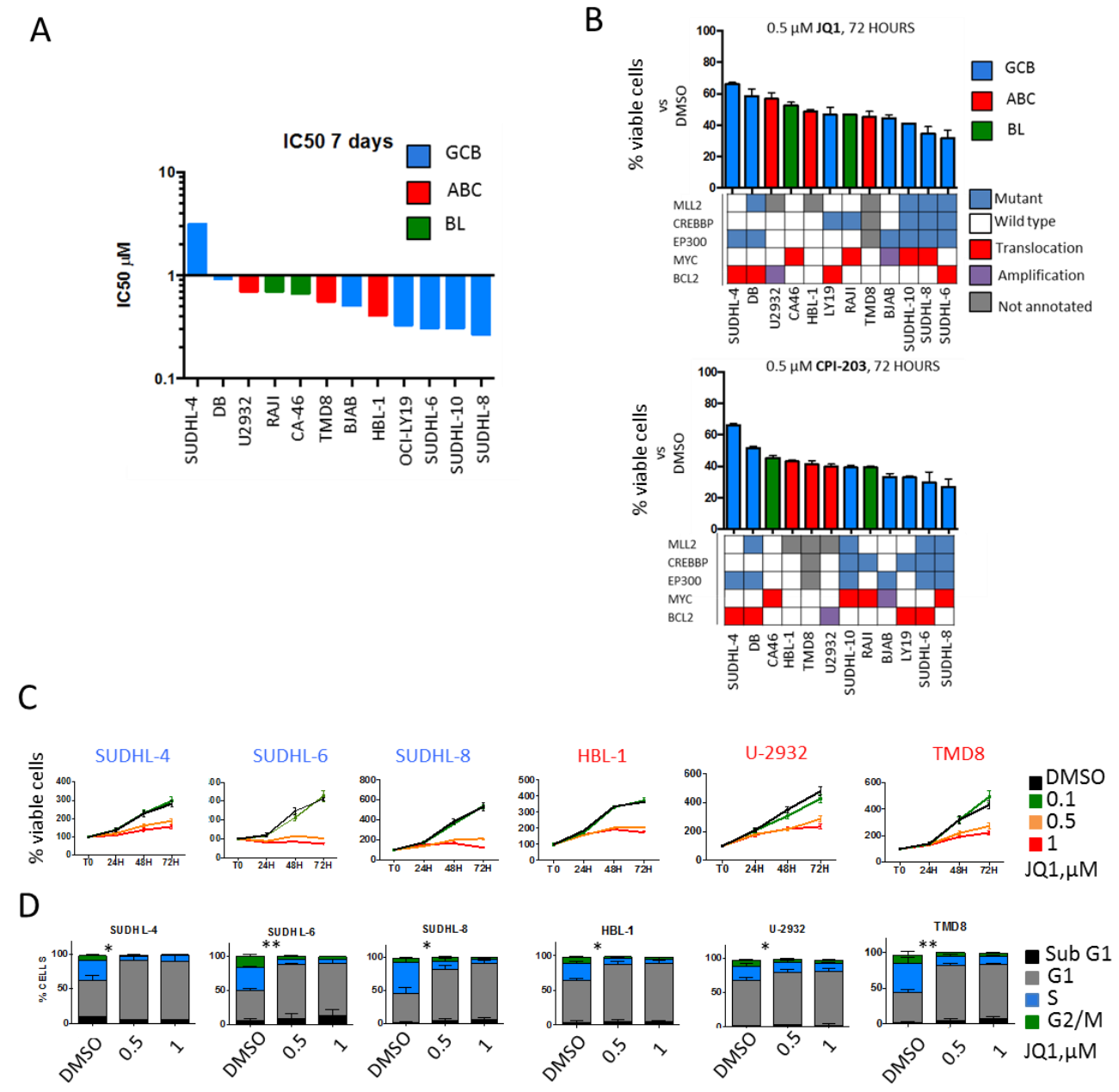
A
IC50 7 days
GCB
ABC
BL
IC50 µM
SUDHL-4
DB
U2932
RAJI
CA-46
TMD8
BJAB
HBL-1
OCI-LY19
SUDHL-6
SUDHL-10
SUDHL-8
B
0.5 µM JQ1, 72 HOURS
% viable cells vs DMSO
MLL2
CREBBP
EP300
MYC
BCL2
Mutant
Wild type
Translocation
Amplification
Not annotated
0.5 µM CPI-203, 72 HOURS
C
SUDHL-4
SUDHL-6
SUDHL-8
HBL-1
U-2932
TMD8
% viable cells
T0
24H
48H
72H
DMSO
0.1
0.5
1
JQ1,µM
D
% CELLS
Sub G1
G1
S
G2/M
JQ1,µM

Figure S1. Antiproliferative activity of JQ1 in aggressive B-cell lymphoma cell lines. Related to figure 1.

A) Bar graph showing 7 day-IC 50 values of our B-cell lymphoma cell line panel (n=12), treated with the bromodomain inhibitor JQ1, in a logarithmic scale. Results are from an automated drug screening assay.

B) Bar graphs showing the efficacy of treatment with JQ1 and CPI-203 0.5 μM for 72 hours in our cell line panel, with respect to the cell of origin and the presence of absence of recurrent mutations of histone modifiers genes, MYC and BCL-2 rearrangements. Viability was determined by MTS assay. Mutations were annotated according to Cancer Cell Line Encyclopedia (http://www.broadinstitute.org/ccle/home), and Pasqualucci et al, 2011; and Zhang et al, 2013. Error bars represent standard error of the mean (S.E.M) of triplicate experiments.

C) MTS assay of 6 representative DLBCL cell lines treated with 0.1, 0.5 and 1 μM JQ1 for 24, 48, 72 hours. Cell viability is plotted vs T0. Error bars represent S.E.M of triplicate experiments.

D) Cell cycle analysis of 6 representative DLBCL cell lines treated with 0.5 and 1 μM JQ1 for 72 hours, showing significant increase in the G1 cell cycle fraction after treatment with JQ1. Error bars represent S.E.M of triplicate experiments. P values were calculated with the Student`s T test * $p< 0.05$, ** $p<0.01$.

Fig. S2

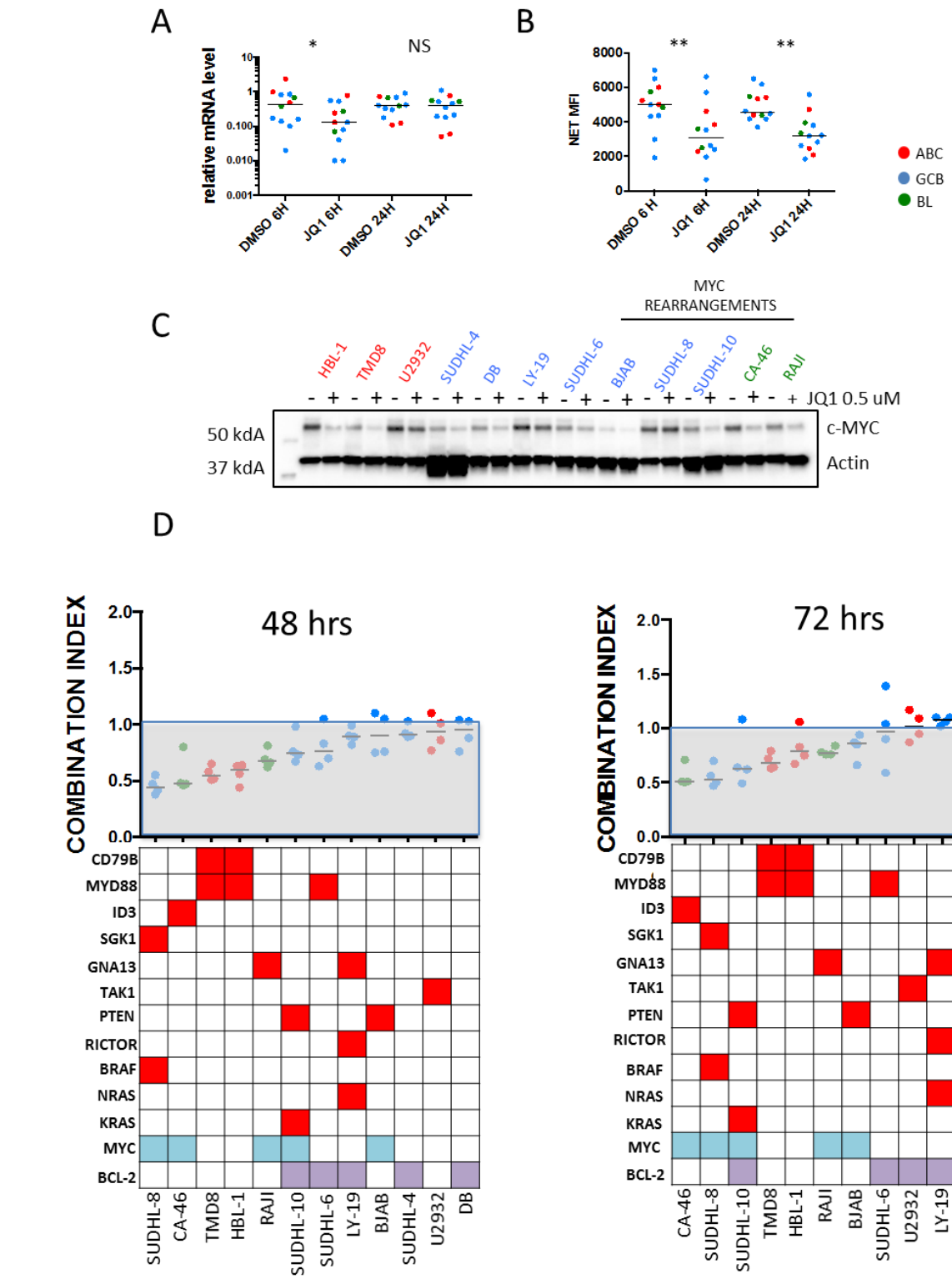
A
relative mRNA level
*
NS
DMSO 6H
JQ1 6H
DMSO 24H
JQ1 24H
B
NET MFI
**
**
ABC
GCB
BL
C
MYC REARRANGEMENTS
HBL-1
TMD8
U2932
SUDHL-4
DB
LY-19
SUDHL-6
BJAB
SUDHL-8
SUDHL-10
CA-46
RAJI
JQ1 0.5 uM
50 kdA
37 kdA
c-MYC
Actin
D
48 hrs
72 hrs
COMBINATION INDEX
CD79B
MYD88
ID3
SGK1
GNA13
TAK1
PTEN
RICTOR
BRAF
NRAS
KRAS
MYC
BCL-2
SUDHL-8
CA-46
TMD8
HBL-1
RAJI
SUDHL-10
SUDHL-6
LY-19
BJAB
SUDHL-4
U2932
DB

Figure S2. JQ1 downregulates MYC and enhances the antiproliferative activity of the PI3K inhibitor BKM-120 in DLBCL and BL cell lines. Related to figure 1.

A) Scatterplot showing the effects of JQ1 on relative *MYC* mRNA levels in our cell line panel. Cells where incubated with JQ1 0.5 μM for 6 and 24 hours and MYC expression levels were assessed by qPCR. P values were calculated with the Wilcoxon Rank test. * $p< 0.05$, ** $p<0.01$.

B) Scatterplot showing the effects of JQ1 on c-MYC protein levels in our cell line panel. Cells where incubated with DMSO or JQ1 0.5 μM for 6 and 24 hours and c-MYC expression levels were assessed by luminex. Mean c-MYC fluorescence intensity levels were normalized to beta tubulin levels. Median c-MYC downregulation at 24 hours across all cell lines was 0.65 (35%). P values were calculated with the Wilcoxon Rank test. * $p< 0.05$, ** $p<0.01$.

C) Representative western blot assay confirming decreased c-MYC expression levels after 6 hours incubation with JQ1 0.5 μM.

D) Scatterplots summarizing the results of our MTS assay validation of the HT screening data at 48 and 72 hrs. Cells were incubated with increasing concentrations (0.25, 0.5, 0.75 and 1μM) of JQ1 and BKM-120, and the combination index was calculated according to the Chou-Talalay method from the average of 3 independent experiments. Genomic alterations of MYC, BCL-2 and genes involved in PI3K and BCR signaling are represented in the heat map. Mutations were annotated according to Cancer Cell Line Encyclopedia (http://www.broadinstitute.org/ccle/home), and Davis et al 2010, Ngo et al, 2011, Fontan et al, 2012

Fig. S3

	CA-46	HBL-1	TMD8	U2932	DB	LY-19	SUDHL-4	SUDHL-6	SUDHL-8
AKT1	4.0	1.1	1.0	1.1	1.4	1.1	1.3	1.3	0.8
AKT2	3.9	1.0	0.8	1.1	1.1	0.7	1.2	1.0	1.1
BAD	2.8	1.0	1.0	0.9	1.0	0.5	1.4	0.8	0.5
BCL2	BD	1.7	2.2	0.9	0.8	1.7	0.4	0.4	0.4
BCL2L1	2.5	1.0	3.2	0.5	0.9	0.8	1.0	0.6	0.7
CASP9	5.5	1.5	1.5	1.3	1.6	1.6	1.6	1.4	1.3
CCND1	BD	0.6	0.5	0.3	BD	BD	BD	BD	BD
CCND2	BD	0.6	1.1	0.4	0.6	0.3	0.3	0.8	0.8
CCND3	0.5	1.0	0.6	1.0	0.9	0.4	0.8	0.6	0.3
CDH1	0.8	BD	2.9	BD	BD	BD	BD	BD	BD
CDKN1A	0.4	1.2	1.1	1.4	2.5	1.6	1.5	1.4	2.1
CHUK	1.3	1.1	1.2	1.1	1.0	1.2	1.1	1.2	1.1
COL1A1	0.3	15.1	1.4	0.8	0.9	0.5	0.6	3.8	1.5
CREB1	1.7	1.2	1.5	1.2	1.6	1.3	1.5	1.3	1.3
CRP	BD	4.9	2.8	BD	0.7	BD	5.3	5.4	3.1
CTNNB1	1.8	1.3	1.5	1.3	1.7	1.3	1.5	1.4	1.4
EIF4EBP1	0.8	0.6	0.5	0.9	0.6	0.7	0.8	0.5	0.8
ELK1	1.1	1.2	1.0	1.1	1.0	1.0	1.0	1.0	0.9
ERBB2	2.0	1.6	1.2	1.3	1.5	1.0	1.1	2.2	1.3
FOS	6.1	2.1	20.9	3.1	1.6	1.8	1.9	5.7	3.4
FOXO3	1.2	1.8	1.5	1.0	1.1	1.5	2.0	1.2	1.6
GRB2	1.6	1.2	1.3	1.2	1.1	1.0	1.1	0.9	1.1
GSK3A	1.3	1.0	1.1	1.0	1.1	0.3	1.1	1.0	0.9
GSK3B	2.2	1.5	2.1	1.6	1.8	2.1	1.9	1.7	2.2
GYS1	1.4	1.4	1.5	1.1	1.2	1.2	1.6	1.5	1.2
HIF1A	1.6	1.0	1.5	1.0	1.5	1.3	1.9	1.6	1.2
HRAS	1.0	0.9	0.9	0.9	0.8	0.7	0.9	0.8	0.6
IGF1	BD	BD	BD	0.2	BD	BD	BD	BD	BD
IGF1R	1.6	1.6	1.7	1.3	0.4	1.6	0.6	1.5	1.2
IGF2	2.5	0.6	4.2	BD	1.1	2.6	5.2	4.5	2.0
IGFBP2	0.1	1.0	0.1	1.0	0.1	0.0	BD	BD	0.1
IGFBP3	BD	BD	BD	2.0	BD	BD	BD	BD	BD
IGFBP4	BD	3.0	1.1	0.6	0.8	0.4	1.5	2.4	0.7
IGFBP5	BD	BD	3.1	BD	0.6	0.0	1.5	5.6	1.0
IGFBP6	0.3	2.8	0.1	0.8	0.4	1.0	0.3	0.2	2.3
IKBKB	1.4	1.0	1.4	0.9	1.1	1.2	1.1	1.4	1.1
IL6	BD	0.4	0.4	BD	BD	BD	BD	BD	BD
IRS1	1.2	0.7	0.5	0.9	0.5	0.7	0.7	0.9	0.6
IRS2	1.3	2.0	1.0	1.3	BD	1.2	0.7	BD	BD
JUN	2.8	1.2	1.3	1.8	1.6	1.5	1.8	3.3	2.9
MAP2K1	1.3	1.5	1.4	1.3	1.3	1.4	1.5	1.3	1.5
MAP2K2	1.6	1.2	1.3	1.2	1.2	1.5	1.3	1.0	1.5
MAP3K5	1.0	0.6	0.7	1.0		1.1	0.9	1.0	1.0
MAPK1	1.6	1.2	1.3	1.1	1.5	1.1	1.4	1.4	1.1
MAPK3	0.4	0.5	0.3	0.5	0.6	0.2	0.5	0.3	0.1
MTOR	1.6	1.2	1.3	1.3	1.7	1.6	1.0	1.2	1.3
MYC	1.0	0.6	0.5	1.1	0.8	0.9	0.6	1.0	1.3
NFKB1	1.5	1.2	3.5	0.8	1.0	0.9	1.2	0.9	1.1
NFKB2	1.5	0.8	2.5	0.6	0.9	1.0	1.2	1.2	1.2
NFKBIA	2.1	1.1	4.8	1.0	2.8	1.1	2.8	1.1	0.9
NFKBIB	0.7	0.6	1.8	0.6	0.6	0.6	0.8	0.6	0.8
NFKBIE	1.2	1.4	2.0	0.5	1.2	1.0	0.9	1.0	0.9
PDPK1	1.8	1.7	1.4	1.5	2.3	1.9	1.3	1.9	1.8
PIK3CA	2.5	1.5	2.1	1.2	1.4	1.5	1.3	2.8	1.8
PIK3CB	1.5	1.4	1.8	1.3	1.2	1.3	1.1	1.3	1.0
PIK3CD	0.9	0.9	1.1	0.6	1.7	0.9	0.8	0.9	0.7
PIK3R1	1.5	1.6	2.1	1.6	1.9	1.3	1.9	1.7	1.4
PIK3R2	1.7	1.1	1.0	1.1	1.4	1.1	1.0	1.0	1.2
PIK3R3	1.1	0.9	1.1	1.1	0.8	1.1	2.7	1.2	0.7
PTEN	1.4	1.2	1.0	0.8	2.2	1.0	1.0	0.7	0.9
PTGS2	BD	1.0	BD	BD	BD	BD	BD	BD	BD
RAF1	1.4	1.1	1.1	1.0	1.2	1.0	1.0	1.1	1.1
REL	2.0	1.8	4.2	1.2	1.1	1.5	1.5	1.5	1.5
RELA	1.3	1.1	1.2	1.2	1.4	1.3	1.3	1.2	1.2
RELB	1.6	1.0	2.4	0.7	1.0	1.1	1.8	1.3	1.0
RHEB	1.2	1.1	1.3	1.0	1.2	1.0	1.0	1.2	0.8
RPS6KA1	1.1	1.0	1.1	0.8	1.1	1.0	1.0	0.9	0.7
RPS6KA2	3.3	2.3	2.2	1.3	0.9	1.7	2.4	0.8	0.8
RPS6KA3	1.4	1.0	1.8	0.9	1.3	1.2	1.0	1.1	0.9
RPS6KB1	1.8	1.1	1.3	1.3	1.3	1.4	1.2	1.5	1.3
SERPINE1	3.1	0.8	BD	1.9	8.1	BD	1.6	2.6	0.9
SHC1	1.1	1.1	0.8	0.8	0.8	1.2	1.2	1.0	1.1
SOS2	2.1	1.9	1.9	1.5	1.5	1.7	1.8	1.9	1.6
SP1	1.0	1.0	0.8	0.9	0.9	0.9	0.7	0.8	0.6
SPP1	1.3	0.6	0.8	19.7	BD	0.2	0.6	BD	1.1
STAT3	2.8	0.7	0.8	1.8	3.0	1.8	1.7	2.3	2.0
TGFB1	1.7	1.4	1.2	1.4	1.4	1.4	1.0	1.4	1.8
TSC1	1.7	1.5	1.7	1.2	2.1	1.4	1.1	1.7	1.4
TSC2	1.9	1.4	1.6	1.5	1.5	1.1	1.8	1.5	1.3
UBA52	0.5	0.8	0.6	0.6	0.5	0.6	0.5	0.4	0.6
UBB	1.6	1.1	1.3	1.2	1.4	1.3	1.5	1.4	1.1
UBC	1.1	1.3	1.4	1.1	1.1	1.4	1.0	1.0	1.3
VEGFA	0.5	0.7	1.3	0.8	0.8	0.7	1.1	0.9	0.9
YWHAB	1.6	1.2	1.3	1.1	1.3	1.0	1.0	1.2	1.1
YWHAE	1.4	1.0	1.1	1.1	1.1	1.1	0.9	1.1	0.9
YWHAZ	1.6	1.3	1.3	1.0	1.2	1.4	1.4	1.3	1.1

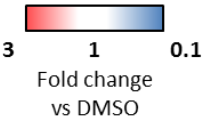

Figure S3. Effect of JQ1 on PI3K pathway gene expression in DLBCL and BL cell lines. Related to figure 2.

Heat map showing fold change values of PI3K pathway components in DLBCL and BL cells after incubation with JQ1 0.5μM for 24 hours. Fold change values of JQ1-treated cells vs DMSO are represented in a colorimetric scale from blue (low) to red (high).

Fig. S4

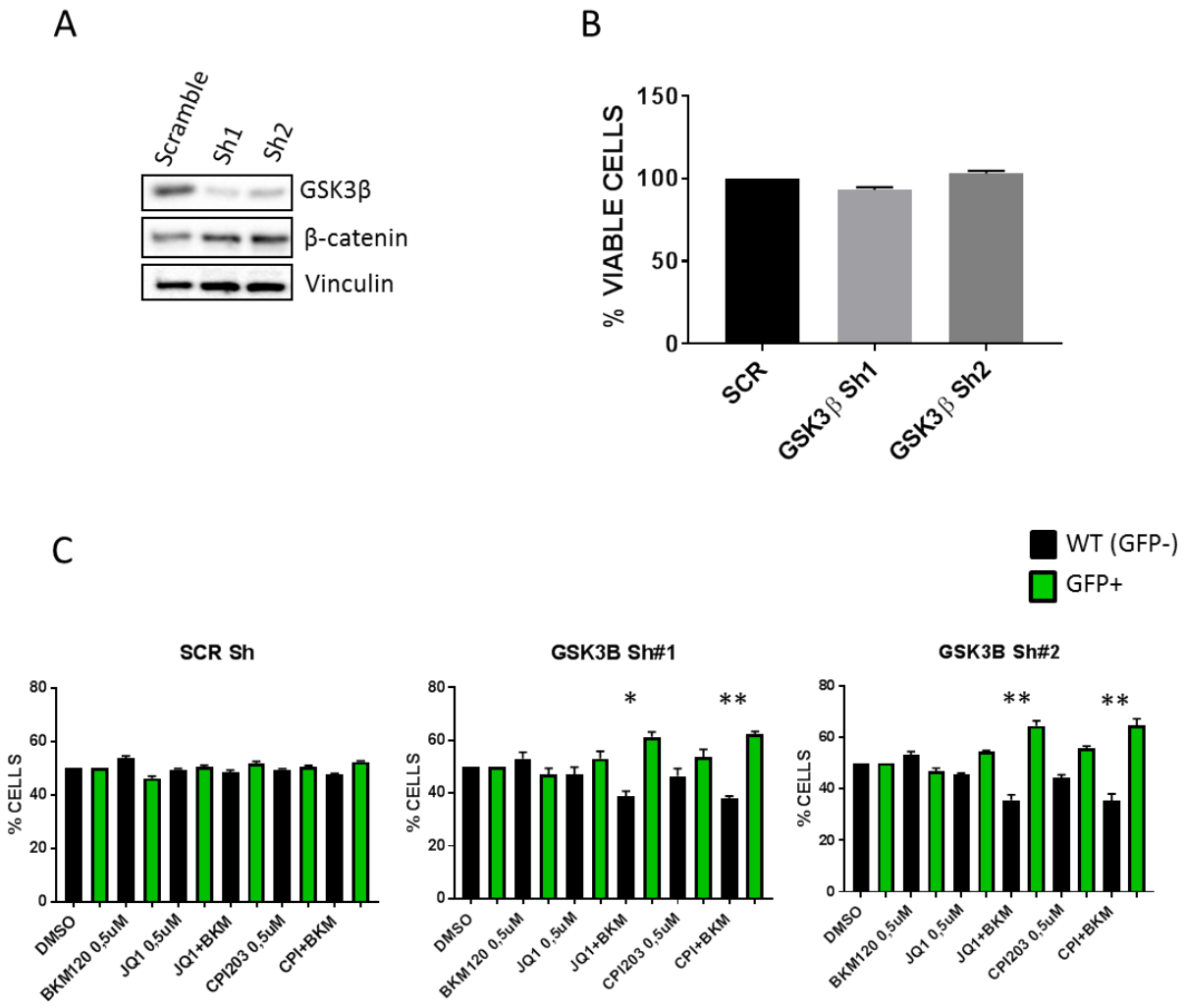

Figure S4. Effects of GSK3β depletion in TMD8 cells. Related to figure 4.

A) Western blot confirming effective *GSK3β* silencing and β-catenin induction after 72 hours of doxycycline (1µg/ml) treatment in TMD8 cells with 2 different *GSK3β* ShRNAs (GSK3β.1, GSK3β.2) vs scramble (SCR).

B) MTS assay showing lack of effect of *GSK3β* silencing on cell proliferation after 72 hours of doxycycline induction in TMD8 cells. Error bars represent S.E.M of triplicate experiments.

A) Bar graphs showing full data of the competitive proliferation assay experiment showed in figure 4F. Briefly, mixtures of GFP positive (scramble, Sh#1 and Sh#2 transduced TMD8 cells) and GFP negative (wild type) cells were induced with 1 µg/ml doxycycline for 72 hours and then incubated with the indicated compounds for additional 72 hours. Then, the % of GFP positive cells in each condition was assessed by flow cytometry. Error bars represent S.E.M of triplicate experiments. Differences between groups (WT vs GFP+ cells) were calculated with the Student T test. * $p< 0.05$, ** $p<0.01$.

Fig. S5


A
MYC-OFF
#1
#2
EXP
MYC
EIF4EBP1
UBA52
PIK3R2
IGF1
MAPK3
GSK3A
MAP2K2
HIF1A
MAPK1
TSC1
UBB
YWHAB
GRB2
RPS6KA3
BAD
PTEN
SHC1
AKT2
SP1
RELA
CCND2
GYS1
UBC
GSK3B
RPS6KA1
REL
CTNNB1
CCND3
NFKB1
PIK3CA
RPS6KA2
CASP9
YWHAZ
CCND1
CREB1
PIK3R1
IKBKB
STAT3
SOS2
RELB
BCL2
PIK3CD
ERBB2
NFKBIE
NFKB2
COL1A1
NFKBIA
CDH1
BCL2L1
IL6
JUN
IGFBP4
5
1
0.1
Fold change
vs DMSO
B
MYC-OFF
30 Min
24 hrs
p-PTEN
p-Akt
p-GSK3-beta
p-GSK3-alpha
p-TSC2
p-mTOR
p-p70S6K
2
1
0.1
Fold change
vs DMSO

Figure S5. MYC dependent regulation of PI3K pathway gene expression and activation in P-4936 cells. Related to figure 5.

A) Heat map showing fold change values of significantly deregulated (>±1.5 average fold change) PI3K pathway-related genes in P-4936 cells after MYC depletion (MYC-OFF), for 24 hours.

B) Effects of MYC silencing for 24 hours (MYC-OFF), on phosphorylation levels of PI3K pathway components, as determined by a PI3K pathway dedicated luminex multiplex assay in P-4936 cells. Average fold change values obtained in 3 independent experiments are represented in a colorimetric scale from blue (low) to red (high).

Fig. S6

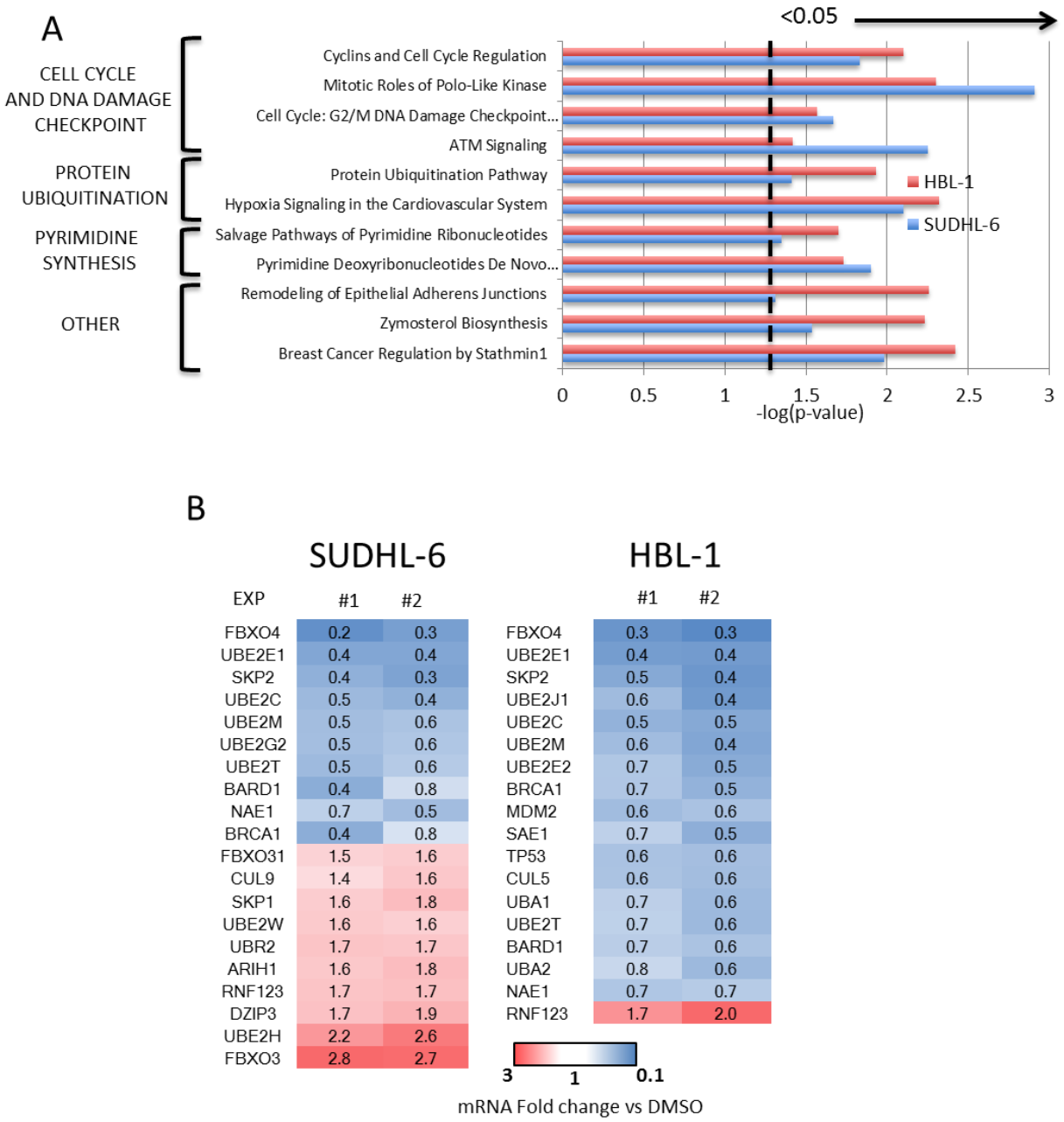

Figure S6. JQ1 deregulates ubiquitination pathway components in DLBCL. Related to figure 6.

A) Ingenuity pathway analysis of SILAC mass spectrometry data showing top 11 commonly regulated pathways in HBL-1 and SUDHL-6 cells after treatment with JQ1 0.5 μM for 24 hours (p-value was calculate with right tailed Fisher`s exact test).

B) Effects of JQ1 on significantly down and upregulated genes (average fold change > +/- 1.5) belonging to protein ubiquitination pathways in SUDHL-6 and HBL-1 cells. Fold change values vs DMSO obtained in 2 independent experiments are depicted in the heat map with a colorimetric scale.

Fig. S7

A

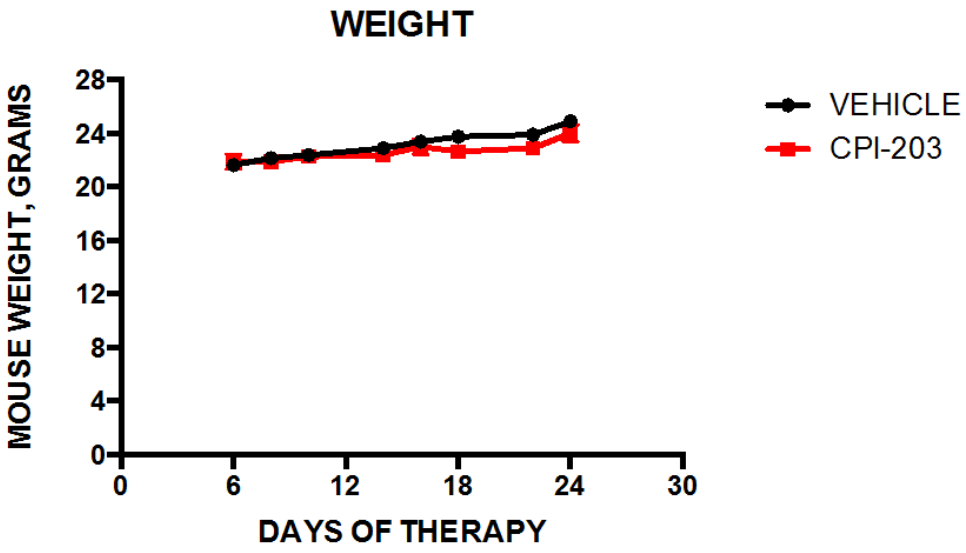
WEIGHT
MOUSE WEIGHT, GRAMS
28
24
20
16
12
8
4
0
0
6
12
18
24
30
DAYS OF THERAPY
VEHICLE
CPI-203

B

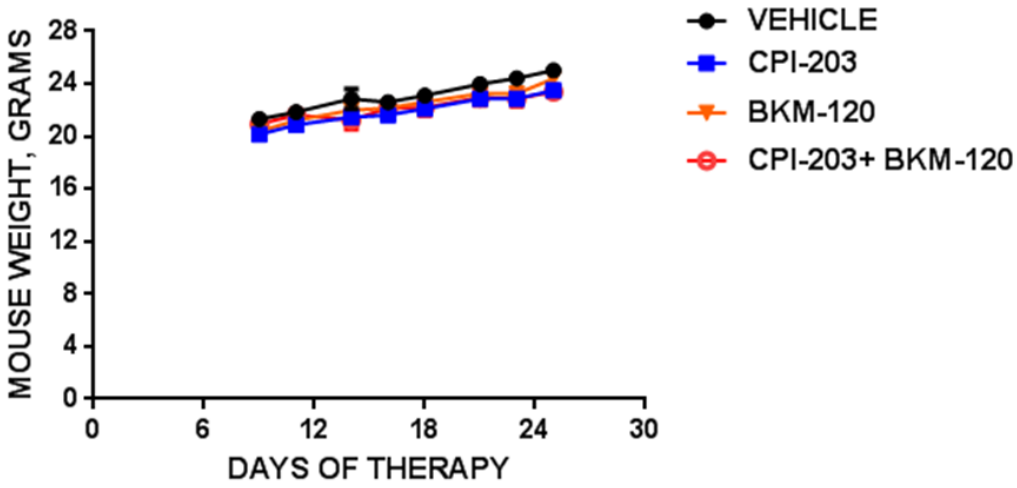
MOUSE WEIGHT, GRAMS
28
24
20
16
12
8
4
0
0
6
12
18
24
30
DAYS OF THERAPY
VEHICLE
CPI-203
BKM-120
CPI-203+ BKM-120

Figure S7. Toxicity of in vivo single agent BET inhibition or combined BET and PI3K inhibition in DLBCL mouse xenografts. Related to figure 7.

A) Graph showing variations of body weight over time in TMD8 xenografts treated with CPI-203 5 mg/kg twice daily.

B) Graph showing variations of body weight over time in TMD8 xenografts treated with vehicle (n=8) CPI-203 5 mg/kg twice daily (n=8), BKM-120 15 mg/Kg daily (n=8), and the combination (n=8).

References (supplementary figures)

Davis RE, Ngo VN, Lenz G, Tolar P, Young RM, Romesser PB, Kohlhammer H, Lamy L, Zhao H, Yang Y, et al. (2010). Chronic active B-cell-receptor signalling in diffuse large B-cell lymphoma. Nature *463*, 88-92.

Fontan L, Yang C, Kabaleeswaran V, Volpon L, Osborne MJ, Beltran E, Garcia M, Cerchietti L, Shaknovich R, Yang SN, Fang F, et al. (2012). MALT1 small molecule inhibitors specifically suppress ABC-DLBCL in vitro and in vivo. Cancer Cell *22*, 812-24.

Ngo VN, Young RM, Schmitz R, Jhavar S, Xiao W, Lim KH, Kohlhammer H, Xu W, Yang Y, Zhao H et al. (2011). Oncogenically active MYD88 mutations in human lymphoma. Nature *470*, 115-9.

Pasqualucci L, Dominguez-Sola D, Chiarenza A, Fabbri G, Grunn A, Trifonov V, Kasper LH, Lerach S, Tang H, Ma J et al. (2011). Inactivating mutations of acetyltransferase genes in B-cell lymphoma. Nature *471*, 189-95.

Zhang J, Grubor V, Love CL, Banerjee A, Richards KL, Mieczkowski PA, Dunphy C, Choi W, Au WY, Srivastava G et al. (2013). Genetic heterogeneity of diffuse large B-cell lymphoma. Proc Natl Acad Sci USA *110*, 1398-403.

Supplemental methods

High-Throughput Drug Screening

Single Agent Dose Response Studies. For the single agent studies, 1 µL of compounds were pre-plated in a 12 point doubling dilution series with 100 µM compound concentration as the upper limit and transferred from an intermediate 384-well polypropylene microtiter plate (Thermo Scientific, Waltham, MA) to a 1536-well microtiter assay plate (Corning, Corning, NY) using the custom-designed 384 head on a PP-384-M Personal Pipettor (Apricot Designs, Monrovia, CA).

For internal reference, each assay plate contained at a final concentration 1% DMSO (v/v) vehicle only as the high control in Row A-B and a 1 uM of killer mix in 1% DMSO (v/v) as the low control in Row EE-FF. To start the assay, cells were seeded at 1,000 cells per well in 8 µL of complete RPMI medium using the FlexDrop IV (Perkin Elmer, Waltham, MA) and incubated for 6 days at 37°C for compound treatment. Next, 1 µL AB was added and further incubated for an additional day at 37°C followed by imaging on the LEADseeker™ Multimodality Imaging System (GE Healthcare, Piscataway, NJ) for resulting fluorescence intensity. Dose response curves for each data set was fitted separately and the two obtained IC_{50} values were averaged for reporting.

***HTS statistical analysis*.** The drugs were tested for activity both as single agents and in combinations on multiple cell lines through the high throughput screening core facility (HTSCF). The residual cell viability post treatment with specific drug combinations was assessed in an Alamar Blue (AB) assay and quantified as fluorescence signal intensity measured using the LEADseeker Multimodality Imaging System (GE Healthcare, Piscataway, NJ). The data was converted into percent inhibitions conferred by each combination relative to both the high (1% DMSO v/v) and the low (1 µM killer mix) control averages (µ). Of note, "killer mix" consists of a HTSCF proprietary mixture of cytotoxic compounds. The percent inhibitions were defined as:

$$\%inhib_i = (\mu_{high\ control} - value_i)/(\mu_{high\ control} - \mu_{low\ control}) \times 100$$

Since the percent inhibition is derived from data measured with error some of the computed numbers can fall outside the [0, 100]% interval. We replaced such valued by the appropriate boundary value. We used the average percent inhibition of the replicates at a dose level (single agent or combination) as the activity at that dose level.

In order to evaluate whether a drug combination shows synergy we compared the observed activity at the combination at that level to the expected activity under Bliss independence model. By treating percent inhibition as a probability and using the product rule for the probability of independent events, the expected activity can be written as

$$P(Inh|A,B) = 1 - P\left(\overline{Inh}\middle|A,B\right) = 1 - P\left(\overline{Inh}\middle|A\right) \times P\left(\overline{Inh}\middle|B\right) = 1 - [1 - P(Inh|A)] \times [1 - P(Inh|B)]$$

where A and B are the two drugs, Inh and $\overline{Inh}$ denote inhibited and not inhibited respectively (Feller, 1971;Tallarida, 2001). The observed can be compared to the expected activity using a simple difference where values around 0 represent additive relationship, large positive values represent synergy and large negative values antagonism. However the same magnitude of the difference represents different relative change depending on the expected activity. Thus we also use a log-odds measure given as $\log\{[P_o(1-P_e)]/[P_e(1-P_o)]\}$ where P_o and P_e are observed and expected activities. For each drug combination we generated a heatmap for the observed inhibition, the difference between observed and expected inhibition and the log-odds of the observed to expected inhibition. The observed and expected inhibition values were rescaled prior to calculating the log-odds by the function (0.8 * observed/expected + 0.1), this was done in order to adjust for instances in which the observed or expected inhibition was 0 or 1. These numbers are binned into intervals suitable for each scale and color coded for simple visualization of the combined activity. For comparing drug combinations we combined the log-odds data across all cell lines and used the medians to rank the combinations. The data are shown as boxplots. All analyses were done using R programming language (R Core Team, 2014).

PCR pathway arrays and qPCR

Total RNA was extracted with the Qiagen (Valencia, CA) RNeasy mini kit protocol. A total of 1 ug of RNA was converted to cDNA using iScript cDNA synthesis kit (Bio-Rad). Real-time polymerase chain reaction (PCR) was performed using the model CFX96 (Biorad). The assay used were the IGF-1 receptor signaling pathway H96 (Biorad), and the human protein ubiquitination H96 panel (Qiagen, PAHS-079Z) according to manufacturer`s instructions. Gene lists for these assays can be found below. For the ubiquitination pathway array reverse transcription was performed using the RT2 first strand cDNA synthesis kit (Qiagen, cat n°330404). Primers for GAPDH, MYC, were purchased from Biorad. GAPDH (qHsaCED0038674), MYC (qHsaCID0012921).

SiRNA experiments

siRNA transfections were performed by using the Amaxa 4D –Nucleofector Unit (Lonza). MYC siRNA: Briefly, $3x10^6$ cells per condition were transfected with 1 μM siRNA or scramble, and resuspended in RPMI 10% FBS with no antibiotics. siRNAs were purchased from Life Technologies (NY, USA): MYC (#4392420: s9129, s9130), Negative Control 1 (#4390643). UBE2C and UBE2T siRNAs: A heterogeneous mixture of small interfering RNAs (siRNAs) that target human UBE2C and UBE2T mRNA sequence were purchased from Dharmacon (Smartpool ON-TARGETplus; L-004693-00-0005 and L-004898-00-005, respectively). Cells were transfected with 25nM and 75nM (per well of a six-well plate) of UBE2C and UBE2T siRNAs or control (scrambled) siRNA. Optimization was done using the Amaxa Cell Line Optimization 4D-Nucleofector X kit (#V4XC-9064). Transfection was performed using the 4D- Nucleofector X kit L (#V4XC-2024).

GSK3β ShRNA experiment

The short hairpin RNA (shRNA) was cloned into the pRSIT17-U6Tet-sh-CMV-TetRep-2A-TagGFP2-2A-Puro Vector (Cellecta), to generate stable lentiviral infected cell lines harbouring a Tet-On inducible Knock Down system.

This vector includes an inducible version of U6 shRNA promoter for Tet regulated shRNA expression, a TagGFP2 mark and a puromycin resistance gene. The shRNA were designed against the coding sequence of *GSK3β*. Sequences are the followings:

SCRAMBLE :
- shRNA for use as a negative control.
Sequence: CCTAAGGTTAAGTCGCCCTCGCTCGAGCGAGGGCGACTTAACCTTAGG

GSK3β Sh#1
Sequence: CCGGCCACAGAACCTCTTGTTGGATCTCGAGATCCAACAAGAGGTTCTGTGGTTTTTG

GSK3β Sh#2
Sequence: CCGGCATGAAAGTTAGCAGAGATAACTCGAGTTATCTCTGCTAACTTTCATGTTTTTG

Western blotting

Preparation of cellular protein lysates was performed by using the Cell Signalling lysis buffer (#9803) according to manufacturer`s extraction protocol. Protein quantitation was done using the Direct Detect system (Millipore).

A total of 30 ug of protein was denatured in Laemli buffer at 95C for 5 minutes and western immunoblotting was performed using the Biorad system (TGX 4-15% gels). Transfer was performed using the Trans Blot turbo system (Biorad) onto PVDF membranes. Images were acquired by using the BioRad Imaging Chemidoc MP system. Secondary anti-rabbit and anti-mouse HRP-conjugated antibodies were purchased from Biorad (#170-6515, #170-6516). The ImageJ software was used to perform densitometry analyses of western blots. Results for each band were normalized to the beta-actin/GAPDH levels in the same blot. The following antibodies for western blotting were purchased from cell signalling technology: PI3Kα (#4249), GSK3β S9 (#9322), GSK3β (#12456), β-catenin (#9582), TUBULIN (#2128). The following antibodies were purchased from Abcam: c-MYC (#32072), PI3K-p85α (#22653), UBE2C (#56861), UBE2T (#140611), lamin B1 (#16048). Beta-Actin (#A5316) and Vinculin (#V9131) were from SIGMA.

Nuclear-cytoplasmic fractionation

For the nuclear and cytoplasmic cell fractionation we used a centrifugation method. To obtain the cytoplasmic fraction, samples were lysed in ice-cold Nuclear Prep buffer (10 mM Tris-HCl pH 8.0, 100 mM NaCl, 2 mM MgCl2, 0,3M Sucrose, 0.2% NP40) plus protease inhibitors (Roche) and centrifugated at 3,000 rpm for 5 min. Subsequently, pellet containing nuclei were lysed in ice-cold S300 buffer (20 mM Tris-HCl (pH 8.0), 300 mM NaCl, 10% glycerol, 0.2% NP40) supplemented with protease inhibitors (Roche), sonicated and centrifugated at 13,000 rpm for 15 min to obtain nucleoplasmic fraction.

Cytokine and chemokine detection

To assess the effects of various treatments on cytokine and chemokine regulation cell lines were incubated with DMSO (0.1%), or different treatments for 24 hours and cell culture supernatants examined with a luminex multiplex assay (#HCYT-MAG-60K-PX41, Millipore), according to the manufacturer's instructions. Samples were run in duplicate and read using the luminex MAGPIX machine. Standard ELISA for MIP-1α was performed using the Quantikine MIP-1α human ELISA kit from R&D Systems, (#DMA00) according to manufacturer`s instructions.

Flow cytometry (Cell cycle analysis)

Cell Staining: Single cell suspensions were prepared and fixed with 70% fresh Ethanol for 2 hrs. After fixation, cells were washed twice with 1x PBS. Cells were then stained with neat (undiluted) Propidium Iodide (PI)/RNase Staining Solution (Cell Signaling, #4087) for 15 minutes at room temperature, protected from light before analysis. **Data Acquisition:** Flow cytometric data was acquired on a BD FACSCalibur (BD Biosciences, San Jose, CA) using CellQuest Pro Version 6.0. Propidium iodide was excited by the 488nm laser and fluorescence emission was measured in fluorescence parameter 3 (FL3) – with the standard 670LP filter. Greater than 10,000 events were acquired. **Data Analysis:** Doublets were excluded by gating out high FL3-W (width) cells.

Xenograft studies

6-week old NSG female mice were injected subcutaneously with 10 million TMD8 cells together with matrigel. Once tumors reached an average volume of 100 mm^3, mice were randomized to receive either vehicle control (5%DMSO/10% hydroxypropylbeta cyclodextrin) or CPI-203 at a dose of 5 mg/kg i.p. twice daily for 3 weeks. Combination experiments were performed in a similar manner: mice were randomized to receive either vehicle control, CPI-203 5 mg/kg i.p. twice daily, BKM-120 15 mg/Kg/daily by oral gavage, or both. Mice were observed daily throughout the treatment period for signs of morbidity/mortality. Tumors were measured three times weekly using calipers, and volume was calculated using the formula: length x $width^2 \times 0.52$. Body weight was also assessed three times weekly. After 3 weeks of treatment tumor samples were collected for immunoblotting.

Mass spectrometry studies data analysis

Lysis and in-situ digestion

The tryptic peptides were desalted by using stage tips (Thermo Scientific) using the manufacturer's instructions. The purified peptides were diluted to 0.1% formic acid, and each gel section was analyzed separately by microcapillary LC with tandem MS by using the NanoAcquity system (Waters) with a 100-inner diameter×10-cm lengthC18 column 1.7µm BEH130; Waters) configured with a 180-µm×2-cm trap column coupled to a Orbitrap Elite mass spectrometer (Thermo Fisher Scientific). Peptides were eluted with a 0-50% linear gradient of Acetonitrile

(0.1% formic acid) / Water (0.1% formic acid) over 200 mins at 300 nL/min. Key parameters for the mass spectrometer were: automatic gain control (AGC) 3×106 ions, resolution 120,000, m/z 300-1650 and a top 10 CID method.

MAXQUANT. All MS/MS samples were analyzed using MaxQuant (Max Planck Institute of Biochemistry, Martinsried, Germany; version 1.3.0.3) at default settings with a few modifications. The default was used for first search tolerance and main search tolerance: 20 ppm and 6ppm, respectively. Labels were set to Arg10 and Lys6. MaxQuant was set up to search the reference human proteome database downloaded from Uniprot on April 2, 2013. Maxquant performed the search assuming trypsin digestion with up to 2 missed cleavages. Peptide, Site and Protein FDR were all set to 1% with a minimum of 1 peptide needed for Identification but 2 peptides needed to calculate a protein level ratio. The following modifications were used as variable modifications for identifications and included for protein quantification: Oxidation of methionine, Acetylation of the protein N-terminus. Carbamidomethyl was used as a fixed modification for Cysteines. Raw data, Uniprot human fasta file as well as original MaxQuant result files can be provided upon request.

Scaffold. Maxquant results were imported into Scaffold Q+S (Proteomesoftware, Portland, Oregon, version 4.4.1). For Scaffold import, all default parameters were used against the same Uniprot human fasta file as searched in Maxquant. Scoring System was LFDR scoring with standard experiment wide protein grouping. Proteins and peptides were filtered at 1% FDR. For Q+S analysis, DMSO samples were organized as the reference channel. The JQ1 samples were organized as Category 1. Q+S normalization was done using the default protein reference.

Prime PCR IGF-1 signaling pathway array gene list

AKT1,AKT2,BAD,BCL2,BCL2L1,CASP9,CCND1,CCND2,CCND3,CDH1,CDKN1A,CHUK,COL1A1,CREB1,CRP,CTNNB1,EGFR,EIF4EBP1,ELK1,ERBB2,FOS,FOXO3,GAPDH,GRB2,GSK3A,

GSK3B,GYS1,HIF1A,HPRT1,HRAS,IGF1,IGF1R,IGF2,IGFBP1,IGFBP2,IGFBP3,IGFBP4,IGFBP5,IGFBP6,IKBKB,IL6,IRS1,IRS2,JUN,MAP2K1,MAP2K2,MAP3K5,MAPK1,MAPK3,MTOR,MYC,

NFKB1,NFKB2,NFKBIA,NFKBIB,NFKBIE,PDPK1,PIK3CA,PIK3CB,PIK3CD,PIK3R1,PIK3R2,

PIK3R3,PTEN,PTGS2,RAF1,REL,RELA,RELB,RHEB,RPS6KA1,RPS6KA2,RPS6KA3,RPS6KB1,
SERPINE1,SHC1,SOS2,SP1,SPP1,STAT3,TBP,TGFB1,TSC1,TSC2,UBA52,UBB,UBC,VEGFA,

YWHAB, YWHAE, YWHAZ

Ubiquitination pathway PCR array gene list

Ubiquitin-Activating Enzymes (E1)

ATG7, MOCS3, NAE1, NEDD8, SAE1, UBA1, UBA2, UBA3, UBA5.

Ubiquitin-Conjugating Enzymes (E2)

Regulation of Apoptosis: BARD1, BRCA1, TP53 (p53), UBE2Z.

Cell Cycle Regulators: ANAPC2, BARD1, BRCA1, CDC34, TP53 (p53), UBE2C, UBE2I.

Transcriptional Regulation: BRCA1, TP53 (p53), UBE2K, UBE2W.

Other Ubiquitin-Conjugating Enzymes (E2): ARIH1, BTRC (bTrCP), NEDD8, PARK2, STUB1, TMEM189, UBA6, UBE2A, UBE2B, UBE2D1, UBE2D2, UBE2D3, UBE2E1, UBE2E2, UBE2E3, UBE2G1, UBE2G2, UBE2H, UBE2J1, UBE2J2, UBE2L3, UBE2M, UBE2N, UBE2Q1, UBE2R2, UBE2S, UBE2T, UBR2.

Ubiquitin-Protein Ligases (E3)

Regulation of Apoptosis: BARD1, BRCA1, CUL1, CUL2, CUL3, CUL4A, CUL5, TP53 (p53), UBE4B, VHL.

Cell Cycle Regulators: ANAPC11, ANAPC2, BARD1, BRCA1, CUL1, CUL2, CUL3, CUL4A, CUL4B, CUL5, CUL7, DDB1, MDM2, CUL9, SKP1, SKP2, TP53 (p53), VHL.

Transcriptional Regulation: BRCA1, CBL, MDM2, SMURF2, TP53 (p53), VHL, WWP1.

Other Ubiquitin-Protein Ligases (E3): ARIH1, BRCC3, BTRC (bTrCP), DZIP3, FBXO3, FBXO31, FBXO4, FBXW10, FBXW9, HECW1, HECW2, HERC5, HUWE1, MARCH5, MIB1, MUL1, NEDD8, PARK2, RFWD2 (COP1), RNF123, RNF148, SMURF1, STUB1, SYVN1, UBE2L3, UBE2T, UBR1, UBR2.

References (supplemental methods)

Feller, W. (1971). An Introduction to Probability Theory and Its Applications. New York, USA. John Wiley&Sons.

R Core Team. R: A language and environment for statistical computing. (2014). R Foundation for Statistical Computing, Vienna, Austria. URL http://www.R-project.org/.

Tallarida RJ. (2001). Drug synergism: its detection and applications. J Pharmacol Exp Ther. *298*, 865-72.